THE JOURNAL OF PHYSICAL CHEMISTRY B
A JOURNAL OF THE AMERICAN CHEMICAL SOCIETY

pubs.acs.org/JPCB Article

# Influence of Magnesium on the Structure of Complex Multicomponent Silicates: Insights from Molecular Simulations and Neutron Scattering Experiments

N. Bisbrouck, M. Micoulaut,* J.-M. Delaye,* M. Bertani, T. Charpentier, S. Gin, and F. Angeli

**Cite This:** *J. Phys. Chem. B* 2021, 125, 11761−11776 Read Online

ACCESS | Metrics & More | Article Recommendations | SI Supporting Information

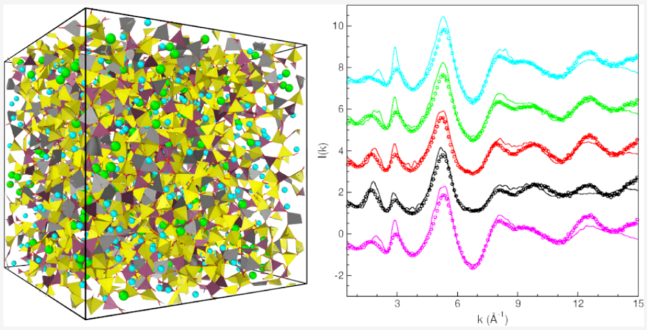

**ABSTRACT:** A series of multicomponent glasses containing up to five oxides are studied using classical molecular dynamics simulations and neutron scattering experiments. The focus is on the role of magnesium in determining the structural properties of these glasses and the possible mixed effect during a sodium/magnesium substitution. Calculated structure functions (pair correlation function and structure factor) rather accurately reproduce their experimental counterpart, and we show that more fine structural features are qualitatively reproduced well, despite some discrepancies in the preferential spatial distribution between sodium and magnesium to aluminum and boron, as well as the nonbridging oxygen, distribution. The simulated systems offer a solid basis to support previous experimental findings on the composition−structure relationship, allowing for further analysis and property calculation. It is confirmed that the substitution of sodium by magnesium leads to the decrease of four-fold boron and a modification of the alkali coordinations with a significant change of the network structure. Specifically, magnesium coordination extracted from numerical simulations highlights a potential dissociation from penta- to tetra- and hexahedral units with increasing MgO contents along the glass series, which could not be resolved experimentally.

## 1. INTRODUCTION

As one of the most abundant element in our universe[1] and in Earth's mantle,[2,3] magnesium has been the subject of increasing interest over the years in various fields such as Earth science wherein the topics on magma transport appear to be central.[4−6] On the other hand, glass has gained tremendous importance in modern society, as emphasized by Morse and Evenson in their title "*Welcome to Glass Age*".[7] Indeed, technological glasses such as borosilicates are commonly used as laboratory glassware,[8] glass cover,[9] or for nuclear waste immobilization.[10−12] In France and in the United Kingdom, part of the borosilicates containing high levels of waste also contains various magnesium contents.[10−14] In medical science, magnesium-containing bioactive glasses can be used for bone repair as magnesium enhances both crystallization and apatite formation at the early stages, which in turn favors contact with living tissues.[15−18] As such, the addition of magnesium to glasses has been studied for some time, and one has found that it intrinsically changes glass properties such as their mechanical behavior,[19−23] glass-transition temperature,[15] viscosity,[21] and chemical durability.[24]

A wide range of experimental characterization techniques can be used to probe the glass structure and help understand the specific role of magnesium in glasses. Its coordination, reflective of its direct environment, is usually found ranging from four to six, as extracted by X-ray diffraction,[25−28] X-ray absorption near-edge structure,[29,30] neutron scattering,[25,26] and indirectly by Raman spectroscopy.[31,32]

$^{25}$Mg solid-state nuclear magnetic resonance (NMR) has also been performed over the years, but only a few results on crystalline or simple glasses are found in the literature,[33−37] with recent results only on borosilicate glasses, as discussed in our previous study,[38] rendering the precise evaluation of the magnesium local environment difficult. Indeed, increasing glass complexity causes higher difficulty in understanding the interactions between magnesium and the other cations, as it varies with the chemical composition.[13,20]

As an alternative analysis technique, molecular dynamics (MD) simulations have been used increasingly over time as an effective tool to observe atomic-level structures of various systems, including multicomponent amorphous and glassy materials.[27,39−44] Typically, simulations can give access to in-depth analysis of data such as bond lengths, bond angles, and

**Received:** August 6, 2021
**Revised:** October 5, 2021
**Published:** October 19, 2021

**Table 1. Nominal Composition of the Studied Glasses, Expressed in Molar Percent of Oxide, Together with the Associated Measured Glass-Transition Temperature ($T_g$), Calculated Fictive Temperature, and Measured Density ($\rho_0$)[a]**

| | chemical composition (mol %) | | | | | | $T_g$ (°C) | | |
|---|---|---|---|---|---|---|---|---|---|
| glass ID | $SiO_2$ | $B_2O_3$ | $Al_2O_3$ | $Na_2O$ | MgO | CaO | measured | simulated | $\rho_0$ (g·cm$^{-3}$) |
| N26M0 | 51.3 | 14.9 | 7.7 | 26.1 | | | 523 | 923 ± 15 | 2.505 |
| N19M8 | 51.2 | 14.9 | 7.7 | 18.7 | 7.5 | | 573 | 916 ± 15 | 2.45 |
| N13M13 | 51.2 | 14.9 | 7.7 | 13.1 | 13.1 | | 594 | 968 ± 15 | 2.421 |
| N8M19 | 51.2 | 14.9 | 7.7 | 7.5 | 18.7 | | 642 | 895 ± 15 | 2.412 |
| N0M12 | 51.3 | 24.2 | 12.4 | | 12.1 | | 703 | 1093 ± 15 | 2.31 |
| N19C8 | 51.2 | 14.9 | 7.7 | 18.7 | | 7.5 | 573 | 944 ± 15 | 2.511 |
| A0B0 | 66.1 | | | 24.2 | 9.7 | | 495 | 1031 ± 15 | 2.486 |

[a] Analyzed compositions are close to nominal compositions taking into account uncertainties and a standard deviation of ±2%.

ring size distributions or oxygen speciation. The method, furthermore, provides insights into the origin of complex and peculiar phenomena such as the mixed-alkali effect in glass.[45,46] However, the reliability of predicted results from simulations is determined by the ability to (re)produce realistic glass systems, which may vary depending on the potentials used. Usually, the first step of numerical studies is the validation of model structures of simulated systems by comparing with experimentally obtained structural data using, for example, neutron or X-ray scattering. As such, the choice of the used potentials will highly depend on the studied properties and systems, with recent comparative studies available.[42,47] This includes composition-dependent partial pairwise potentials[48] or empirical interatomic potentials, as used in this study.[41] Boron potentials for borosilicates were only introduced recently[41,49−51] due partly to the difficulty to reproduce changes in boron coordination depending on the composition, among different parameters. However, while only Wang et al.[41] potentials contained parameters including both boron and magnesium, which are key elements, at the beginning of the study, new potentials have been developed[48,52,53] recently including both species.

The present study follows an in-depth experimental structural characterization of seven glasses (with three to five oxides) of the form $SiO_2$−$B_2O_3$−$Al_2O_3$−$Na_2O$−(MgO, CaO) for the most complex ones, five of which containing magnesium, with the addition of a calcium counterpart to one of the glasses.[38] The whole series was simulated by classical MD using the Wang et al. potential.[41] In parallel, neutron scattering measurements were performed on five glasses to obtain the structure factor $S(k)$, which was compared to the calculated functions as a means to evaluate their relevance and accuracy. Structural data were then obtained on the overall network and compared when possible to previously obtained experimental data. The central findings indicate a relatively good agreement between the major structural features observed experimentally and simulated by MD.

## 2. METHODS

### 2.1. Glass Composition.

In our previous study,[38] we characterized experimentally using multinuclear NMR analysis and Raman spectroscopy seven silicate glasses, which are divided as follows: four magnesium-containing aluminoborosilicate glasses (N19M8, N13M13, N8M19, and N0M12), a complementary calcium-containing glass (N19C8), a sodium aluminoborosilicate glass (N26M0), and a simple reference silicate glass (A0B0). Glass names and compositions are given in Table 1, wherein N and M represent the nominal rounded concentration (mol %) of $Na_2O$ and MgO, respectively. In order to study the impact of magnesium on the studied glasses, the Si/Al and Si/B ratios were maintained constant, except for the sodium-free glass for which Si/Al and Si/B were decreased by 30% to allow the synthesis of a homogeneous structure (partly crystalline structures were observed in the two glasses with a high magnesium content). Magnesium was substituted for sodium in four glasses and was fully substituted for calcium in the N19C8 glass, as a comparison between the two alkali-earth samples. Finally, a simple reference ternary glass without aluminum or boron, A0B0 ($SiO_2$−$Na_2O$−MgO), was also prepared. Detailed synthesis processes are reported elsewhere.[38] In brief, glasses were prepared from analytical-grade oxide and carbonate, with a $^{11}$B enrichment of 99.62%, following a classical melt-quench protocol, with a second fusion to ensure homogeneity.

### 2.2. Simulation Methods.

MD simulations were performed for all glasses with the LAMMPS package[54] using a recent Coulomb−Buckingham-type interatomic potential developed by Wang et al.[41] based on an earlier work by Guillot−Sator.[55] These two-body potentials contain short-range interactions of the form of a repulsive exponential term coupled to an attractive dispersive one, in addition to long-range Coulombic interactions, expressed in eq 1

$$U_{ij}(r_{ij}) = \frac{z_i z_j}{r_{ij}} + A_{ij}\exp\left(-\frac{r_{ij}}{\rho_{ij}}\right) - \frac{C_{ij}}{r_{ij}^{\ 6}} \tag{1}$$

where $r_{ij}$ is the interatomic distance between atoms $i$ and $j$, $z_i$ and $z_j$ are the partial charges of atoms $i$ and $j$ respectively, and $A_{ij}$, $\rho_{ij}$, and $C_{ij}$ are the short-range potential parameters for the $ij$ pairs.

Additionally, a short-range, highly repulsive term (eq 2) is added to avoid spurious effects due to a dramatically strong attraction occurring at a low interatomic distance and a high temperature.[40,56]

$$U_{ij}(r_{ij}) = \frac{B_{ij}}{r_{ij}^{\,n_{ij}}} + D_{ij} r_{ij}^{\ 2} \tag{2}$$

where $B_{ij}$, $n_{ij}$, and $D_{ij}$ are parameters fitted to allow continuity in the force, the potential, and the first derivate of the force at the distance where the second derivate of the force is close to zero.

The simulated systems are composed of randomly generated 5000-atom cubic boxes with periodic boundary conditions and a density equal to the measured experimental ones (herein in Table 1 and reported elsewhere). A cutoff of 10 Å was used for short- and long-range interactions. For the latter, an Ewald summation with a defined accuracy of $10^{-5}$ was performed. A 1 fs timestep was used for all simulations. First, an equilibration step in the *NVT* ensemble (i.e., constant number of atoms, volume, and temperature) was performed for 0.1 ps at 1000 K to remove the initial most energetic interactions. Afterward, the systems were heated to 3000 K in the *NVT* ensemble for 1 ns to ensure the total loss of the initial configuration and then quenched at a 2 K/ps rate to 300 K. Finally, two 20 ps equilibration steps were performed: one in the canonical ensemble, followed by another one in the microcanonical *NVE* ensemble (i.e., constant number of atoms, volume, and energy). A typical simulation box is illustrated in Figure 1.

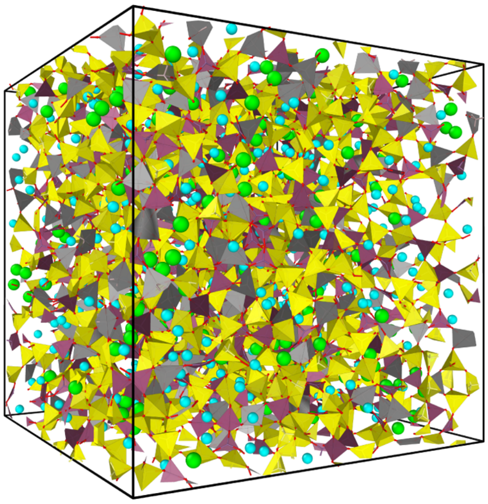

**Figure 1.** Typical snapshot of the 5000-atom N13M13 system containing Mg (green) and Na (cyan) atoms. The network structure made of Si (yellow), O (red), B (purple), and Al (gray) is represented by their atoms, bonds, and polyhedra.

*2.2.1. Fictive Temperature.* The evolution of the system during the quenching is presented in Figure 2, and it reproduces the salient features of the glass transition,[56−58] that is, at a given quenching rate, one obtains a linear behavior in the supercooled state, followed by a break in the slope at a numerical glass-transition temperature $T_g$ or fictive temperature. Here, from the total energy $E(T)$ of the system, $15RT/2$ is subtracted, which corresponds to the harmonic motions in the glassy state. The $T_g$ was estimated following the methods proposed in refs 56 and 59. Values of this fictive temperature (Table 1) were calculated for all systems from the intersection between the two straight lines defining the low- and high-temperature regions. These values greatly exceed the experimental $T_g$ usually observed for numerically determined characteristic temperatures of the glass transition.[56,60] It has been shown by Deng and Du[60] that for a quenching rate of 2 K/ps, the difference between the experimental and simulated $T_g$ of $3Na_2O-B_2O_3-6SiO_2$ is around 700−800 K with the same type of potentials. In our systems, the difference is usually smaller (300−400 K) except for the silica-rich glass (66.1 mol %) A0B0, for which the gap is around 550 K, which is closer to what has been found by Deng and Du in their study. However, it is important to highlight the fact that this calculated $T_g$ is quenching rate-dependent, as well as rigidity-dependent, as the relaxation time needed to achieve equilibrium is higher for more rigid systems.

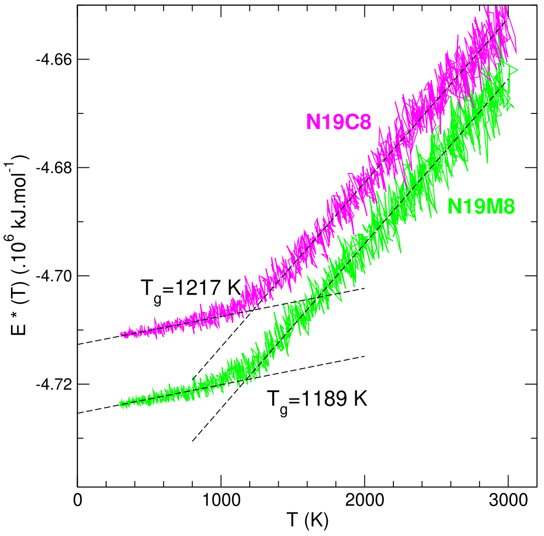

**Figure 2.** Representation of the total energy $E^*(T) = E(T) - 15RT/2$ of two selected systems as a function of temperature, at the same 2 K·ps$^{-1}$ quenching rate. The intersection between the low- and high-temperature behavior (broken lines) defines the fictive temperature.

*2.2.2. Pair Distribution Function, Structure Factors, and Structural Analysis.* The pair distribution function (PDF) $g(r)$ is defined as the probability density of finding any two atoms at a given interatomic distance $r$. Due to the usually limited momentum transfer range accessible experimentally ($k < k_{max}$), and in order to be consistent with the experimental methodology, the calculated PDFs have been convoluted by a normalized Gaussian distribution with a full-width at half-maximum of $5.437/k_{max}$, with a maximum wave vector $k_{max}$ = 20 Å$^{-1}$. This allows for a direct and meaningful comparison with experimental results,[41,61] as also emphasized in other simulation studies.[40,42,47] The partial ($S_{ij}(k)$) and total ($S(k)$) structure factors were calculated from a Fourier transform of the partial PDFs obtained from

$$S_{ij}(k) = 1 + \rho_0 \int 4\pi r^2 [g_{ij}(r) - 1] \frac{\sin(kr)}{kr} \mathrm{d}r \tag{3}$$

$$S(k) = \left( \sum_{i,j=1}^{n} c_i c_j b_i b_j \right)^{-1} \sum_{i,j=1}^{n} c_i c_j b_i b_j S_{ij}(k) \tag{4}$$

where $k$ is the scattering vector, $\rho_0$ is the average atomic density, $c_i$ and $c_j$ are, respectively, the fraction of $i$ and $j$ atoms (herein, Si, O, B, Na, Al, Ca, and Mg) and $b_i$ and $b_j$ are the neutron scattering length of different species, taken as 4.1491, 5.803, 6.65, 3.63, 3.449, 4.70, and 5.375 fm for Si, O, B, Na, Al, Ca, and Mg, respectively.[62]

From the partial pair correlation functions, the coordination number (CN) of atoms is obtained by integration of the partial cation−oxygen (or in other cases, cation−cation) PDF with a cutoff value defined by the first minimum of the PDF. In order to access the topological medium-range order (MRO), we have evaluated the rings' statistics for all compositions from the rigorous investigation of networks generated using simulation (RINGS) code.[63] The cutoff distance has been chosen to be the same as the one used for the coordination number analysis. The ring statistics algorithm is mostly based on the King−Franzblau[64,65] shortest path search to find rings containing a maximum of 20 atoms. In addition, rings can be defined as the shortest closed paths within the network, with the size defined by the number of Si, Al, or B atoms.

**2.3. Neutron Diffraction Experiments.** Neutron diffraction experiments were conducted on five representative $^{11}$B-enriched glasses since $^{10}$B (19.9% abundance) absorbs neutrons. The neutron diffraction measurements were carried out under ambient conditions on the 7C2 diffractometer[66] at the Orphée Léon Brillouin Reactor (France). A neutron wavelength ($\lambda$) of 0.58 Å was selected for the measurements. Powdered glass samples (8 mm in diameter and 5 cm in height, in a vanadium sample holder) were placed into a vacuum chamber. The structure factors were obtained using the program CORRECT,[67] which corrects the data for attenuation, background, multiple scattering, and inelasticity (Placzek) effects. Finally, the total PDFs were then calculated from the structure factors by the Fourier transform[68−71]

$$G(r) - 1 = \frac{1}{2\pi^2 r\rho_0}\int_0^\infty k[S(Q) - 1]\sin(kr)F_L(k)\mathrm{d}k \qquad (5)$$

with $\rho_0$ being the atomic number density and $F_L(k)$ the Lorch[72] correction function accounting for the effect of the finite $k$ in reciprocal space.

## 3. RESULTS

### 3.1. Neutron Scattering and Comparison with MD.

*3.1.1. Structure Factors.* Prior to a full analysis of the atomic scale, it is important to check the relevance of the MD model and to compare the overall structural features with experimental data. This can be achieved by calculating and comparing the structure factor data, presented in Figure 3a.

Three principal peaks (PP) are detected around $k_1$ = 1.70, $k_2$ = 2.95, and $k_3$ = 5.30 Å$^{-1}$ from neutron scattering experiments, with two additional minor contributions at 8.0 and 12.5 Å$^{-1}$. It is important to emphasize that simulations reproduce fairly well the scattering results and display an overall good agreement with experimental data. Slight differences in the first peak position and amplitudes do appear, however. While the exact nature of the first peak contributions remains debated and is thought to be the result of various contributions from partial structure factors, it is generally admitted to be the signature of MRO.[73,74] The discrepancies might indicate that in the present investigated composition range, the MRO might be insufficiently reproduced with increasing sodium content. This situation was observed for all glasses as opposed to results obtained by Wang et al.[41] A decomposition into partials indicates that all structure factors are dominated by O−O, Si−O, and B−O correlations, the other main contributions overall resulting indeed from cation−oxygen interactions, the contributions from cation−cation correlations being negligibly small. The partial structure factor of glasses displayed in the Supporting Information (Figure S1) indicates that sodium contributions might be at the origin of the first peak shift toward a higher $k$, resulting mainly from Na−O interactions, followed mostly by Si−Na and B−Na, and finally lesser contributions from Na−Na and Al−Na.

An additional way to compare both experimental and simulation data is to represent the interference function $I(k) = k[S(k) - 1]$ (Figure 3b) which blows up oscillations in the long wavenumber limit $k$ and provides some information about the accuracy of short range in the real space.[75] Here, the agreement of our simulations is found to be good as fluctuations and minor contributions at 8.0 and 12.5 Å$^{-1}$ are correctly reproduced. It, furthermore, permits highlighting the presence of another peak around 9.9 Å$^{-1}$ that is barely visible from an inspection of $S(k)$ alone. Such minor contributions are usually associated with correlations between secondary shells of neighbors.[76]

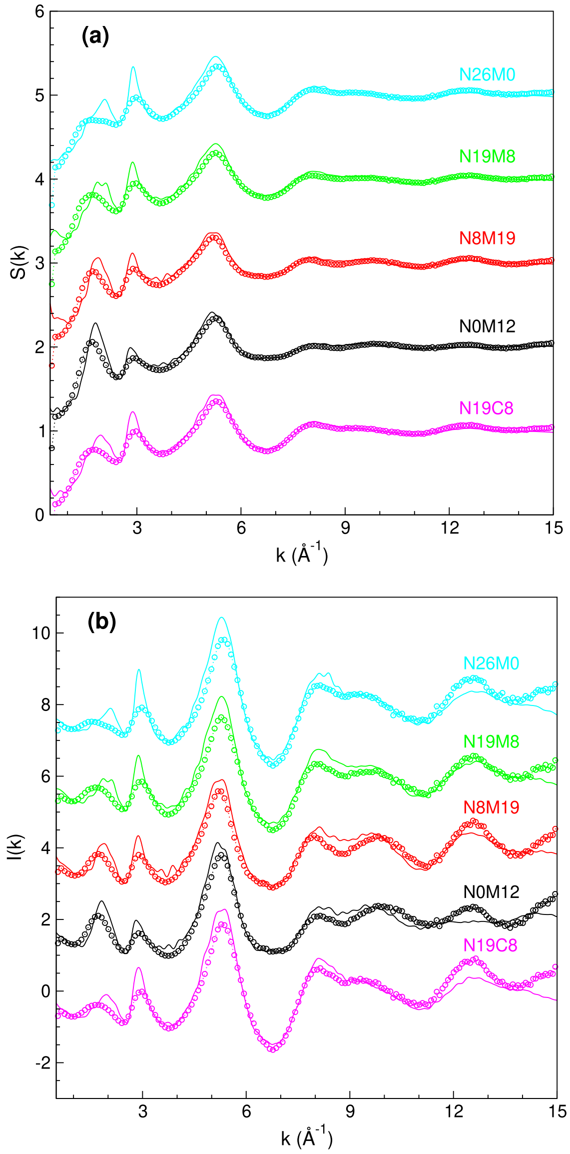

**Figure 3.** (a) Experimental (symbols) and calculated (solid lines) neutron scattering total structure factor $S(k)$ and (b) associated interference functions $I(k)$. Curves have been shifted by multiples of 1.0 for clarity.

As the magnesium content is increased, the first peak becomes narrower and more intense, with a shift in the maximum location toward a higher $k$ (experimentally, from 1.6 Å$^{-1}$ for N26M0 to 1.7 Å$^{-1}$ for N8M19). As calcium is substituted by magnesium, a slight broadening accompanied by a decrease in intensity is observed for the first peak at $k_1$, which indicates a substantial effect on the MRO of magnesium-rich glasses compared to the calcium-rich ones. Finally, among all glasses, the sodium-free glass N0M12 displays the narrowest peak with the highest intensity. In a similar way, increasing magnesium content in the glass series induces a decrease in the second peak intensity $S(k_2)$, accompanied by little to no effect on the third peak and conversely the highest minimum value around 7.0 Å$^{-1}$. Interestingly, the double contribution of peaks around 8.0 and 9.9 Å$^{-1}$ displays major variations with increasing magnesium content. In this region, the first peak, of the highest intensity for N26M0, progressively decreases to the benefit of the second peak that might be related to the increasing presence of Mg−O interactions at the expense of Na−O interactions.

*3.1.2. Pair Distribution Function.* In addition to the information given by neutron scattering in Fourier space, it is insightful to study the effect of cation substitution on the short-range structural order (i.e., on the $g(r)$, see Figure 4) and on the MRO. Due to the limitation of the used $k_{max}$ = 20 Å$^{-1}$, B−O, Si−O, and Al−O contributions are not clearly distinguishable and merged in a single main peak centered around 1.61 Å for most glasses. This is found for all compositions except for N0M12, which displays a main peak at around 1.48 Å. For the latter, the large broadening of the peak coupled to a shift toward a maximum value centered at 1.48 Å can be explained by its highest boron content and B$^{III}$/B$^{IV}$ ratio compared to all the other glasses (see below). Overall, it seems that the first peak intensity decreases with increasing Mg content, and a small broadening occurs. A distinctive shoulder is detected on the second main peak at ≃2.10 Å and appears to depend on the Mg content. Finally, the effect of Ca and Na contents cannot be distinguished as both N19C8 and N19M8 display a similar profile for the function $g(r)$. Due to the major overlapping of partial contributions for $r$ > 4 Å, experimental information is hardly accessible. On the whole, we observe a good agreement between simulated and experimental PDFs, with mainly slight variations in intensity at several distances. The shoulder around 2.04 Å in N8M19 does not appear in the simulation due to the substantial broadening used, allowing for the comparison. Otherwise, this shoulder is well defined, which is representative of the higher resolution achieved by MD. Interestingly, the accuracy of the intensity of the first peak decreases with increasing magnesium content, probably partly due to the variation in B$^{III}$ CN compared to experiments, as discussed later. However, it confirms a short-range structure that is qualitatively reproduced.

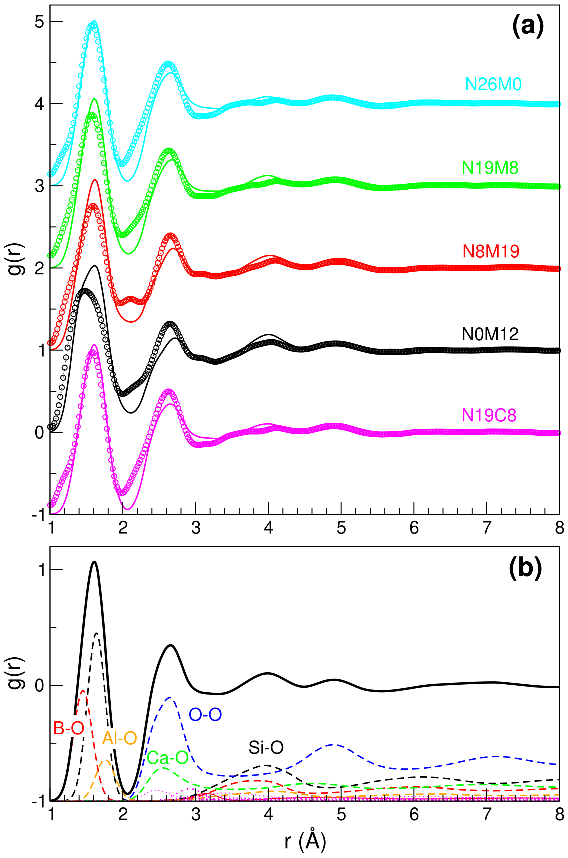

**Figure 4.** (a) Experimental data (symbols) from neutron scattering and calculated (solid curves) total pair correlation function $g(r)$ for the various investigated glasses. (b) Decomposition into appropriately weighted partials (broken lines) is given for the N19C8 glass with indication of the major partial contributions: Al−O, B−O, Si−O, Ca−O, and O−O.

An additional means to decode further the effect of Mg content on the structure builds on the partial correlations. Computing the partial cation−oxygen PDFs allows for both a comparison between the X−O bond lengths (X = Si, Al, B, Mg, Ca, and Na), as well as the CN of all the studied species. These partial PDFs are displayed in Figure 5, and the corresponding bond lengths are listed in Table 2. It is important to note that for a given X−O pair, X−BO, and X−NBO reported values are mean bond distances, while the X−O value denotes the most probable bond distance, that is, at the maximum of the $g(r)$. For all glasses, regardless of the composition, the Si−O bond length is found at around 1.63 Å, which is consistent with the experimental and simulated results on several other systems for tetrahedral silicon units,[40−42,47,77,78] indicating that the tetrahedral $SiO_{4/2}$ can be regarded as a rigid geometrical unit. Al−O distances are found to be about ≃1.75 Å for all glasses, in agreement with other studies.[79,80] Tri- and tetra-coordinated B bond lengths are found to be around 1.40 and 1.47 Å, respectively. These results are in agreement with experimental and MD data.[41,42,47,81−84] Alkali− and alkali-earth−oxygen bond lengths usually display a broad range of values due to their less well-defined environments. As such, the bond lengths of Na−O (experimental values between 2.30 and 2.62 Å),[78,85,86] Ca−O (experimental values between 2.37 and 2.49 Å),[87−90] and Mg−O (experimental values between 1.90 and 2.08 Å)[27,36,39,87,88,91,92] are all consistent with data published elsewhere. For these elements, further investigation of their coordination shell is needed and will be discussed below.

**3.2. Structural Contributions from MD.** *3.2.1. Coordination Analysis.* All cation−oxygen mean CNs are listed in Table 3. As expected, all silicon atoms are found in four-fold tetrahedral units, in good agreement with experimental results of glassy silicates. Aluminum mean CN calculated by MD is slightly larger than 4 in all systems, for example, for N8M19, $n_{AlO}$ = 4.06. It should be noted that these values depend on the chosen cutoff in the corresponding correlation function (i.e., at the minimum), which does not display a global minimum (i.e., $g_{ij}$ = 0) as for Si−O correlations. Regardless of the variability of $n_{AlO}$ induced by the cutoff, it appears that the number of over-coordinated Al$^{V}$ is always 2−3% higher for all magnesium-containing glasses compared to the calcium-containing one (N19C8). This signals a rather generic trend, indicating that the formation of Al$^{V}$ is promoted when magnesium is present in the glass. However, previous NMR results did not indicate a clear increase in penta- and hexa-coordinated aluminum population in the series except for the N0M12 glass.[38] Other

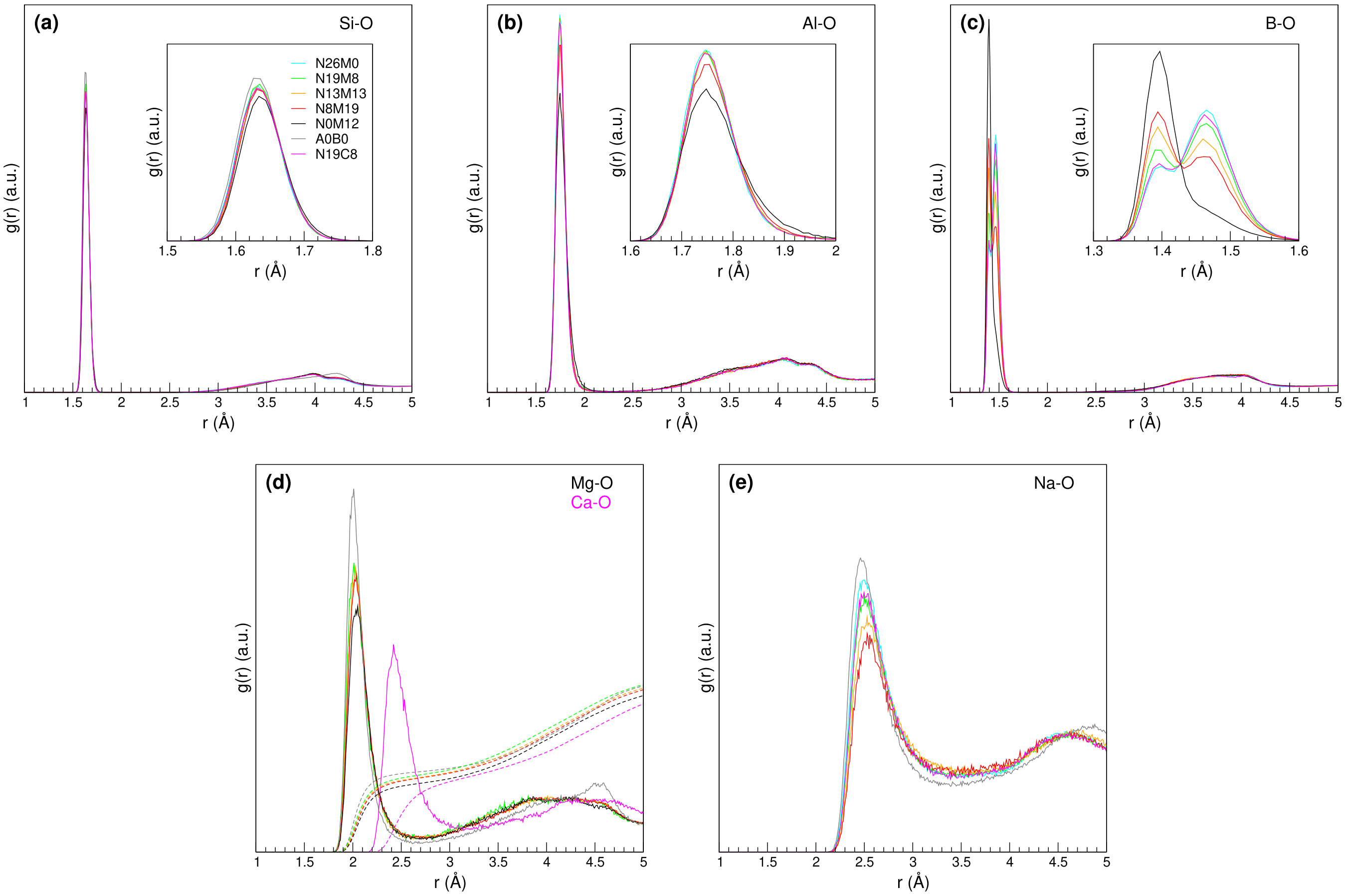

**Figure 5.** Partial PDFs for all glasses. Only the first neighbor correlation (i.e., those involving oxygen) is displayed here. Dashed lines in (d) denotes the integration of the PDFs for magnesium and calcium, respectively, indicative of the CN distribution.

### Table 2. Simulated Cation−Oxygen Bond Length for All Glasses[a]

| | $r_{i-j}$ (Å) | N26M0 | N19M8 | N13M13 | N8M19 | N0M12 | A0B0 | N19C8 |
|---|---|---|---|---|---|---|---|---|
| Si−O | | 1.63 | 1.63 | 1.63 | 1.63 | 1.63 | 1.63 | 1.63 |
| | $r_{BO}$ | 1.64 | 1.64 | 1.64 | 1.64 | 1.64 | 1.64 | 1.64 |
| | $r_{NBO}$ | 1.62 | 1.62 | 1.62 | 1.63 | 1.63 | 1.62 | 1.62 |
| Al−O | | 1.75 | 1.75 | 1.75 | 1.75 | 1.75 | | 1.75 |
| | $r_{BO}$ | 1.76 | 1.76 | 1.76 | 1.76 | 1.75 | | 1.75 |
| | $r_{NBO}$ | 1.73 | 1.74 | 1.74 | 1.75 | 1.75 | | 1.72 |
| $B^{III}$−O | | 1.40 | 1.39 | 1.39 | 1.40 | 1.40 | | 1.39 |
| | $r_{BO}$ | 1.40 | 1.40 | 1.40 | 1.40 | 1.40 | | 1.40 |
| | $r_{NBO}$ | 1.39 | 1.39 | 1.39 | 1.39 | 1.39 | | 1.39 |
| $B^{IV}$−O | | 1.47 | 1.47 | 1.46 | 1.46 | 1.47 | | 1.46 |
| | $r_{BO}$ | 1.47 | 1.47 | 1.47 | 1.47 | 1.47 | | 1.47 |
| | $r_{NBO}$ | 1.45 | 1.46 | 1.46 | 1.46 | 1.45 | | 1.45 |
| Na−O | | 2.49 | 2.50 | 2.53 | 2.54 | | 2.46 | 2.42 |
| | $r_{BO}$ | 2.74 | 2.75 | 2.76 | 2.77 | | 2.80 | 2.75 |
| | $r_{NBO}$ | 2.59 | 2.61 | 2.64 | 2.64 | | 2.61 | 2.60 |
| Mg\Ca−O | | | 2.04 | 2.06 | 2.08 | 2.05 | 2.07 | 2.42 |
| | $r_{BO}$ | | 2.22 | 2.23 | 2.23 | 2.20 | 2.33 | 2.64 |
| | $r_{NBO}$ | | 2.04 | 2.06 | 2.08 | 2.05 | 2.07 | 2.44 |

[a] Backslash (\) denotes either Mg or Ca when applicable.

species such as tri- and tetra-coordinated boron CN change the most through the series of considered glass as in other multicomponent silicates and here appear to decrease with increasing magnesium content. While simulations usually overestimate (or underestimate) the fraction of four-fold boron[42,47] depending on the composition range, the trend is qualitatively well reproduced, as one can see in Figure 6. Particularly interesting is the distinct effect of magnesium compared to calcium on the boron coordination that is well reproduced. This will be discussed later.

The environment of sodium (Na−O) appears similar between N19M8 and N19C8 glasses, with a noticeable

**Table 3. CNs of Each Cation−Oxygen Pair, alongside MD, Yun, Dell, and Bray (YDB),[93,94] and NMR Four-Fold Coordinated Boron Percentages, as Well as Experimental Al CN of All Glasses**

| | Si−O | Al−O | B−O | Na−O | Mg−O | Ca−O | $B^{IV}$ (%) | | | Al NMR CN (%) | | |
|---|---|---|---|---|---|---|---|---|---|---|---|---|
| cutoff (Å) | 2.0 | 2.3 | 2.0 | 3.5 | 2.7 | 3.2 | MD | YDB | NMR[38] | $Al^{IV}$ | $Al^{V}$ | $Al^{VI}$ |
| N26M0 | 4.00 | 4.05 | 3.72 | 7.85 | | | 71.6 | 72 | 57 | 100 | | |
| N19M8 | 4.00 | 4.06 | 3.65 | 7.55 | 5.07 | | 64.6 | 71 | 37 | 100 | | |
| N13M13 | 4.00 | 4.05 | 3.56 | 7.58 | 4.96 | | 55.6 | 36 | 24 | 100 | | |
| N8M19 | 4.00 | 4.06 | 3.48 | 7.21 | 5.04 | | 48.1 | 0 | 7 | 100 | | |
| N0M12 | 4.00 | 4.06 | 3.19 | | 4.83 | | 18.8 | 0 | 2 | 78 | 16 | 6 |
| A0B0 | 4.00 | | | 6.97 | 4.78 | | | | | | | |
| N19C8 | 4.00 | 4.03 | 3.70 | 7.68 | | 7.39 | 69.9 | 71 | 46 | 100 | | |

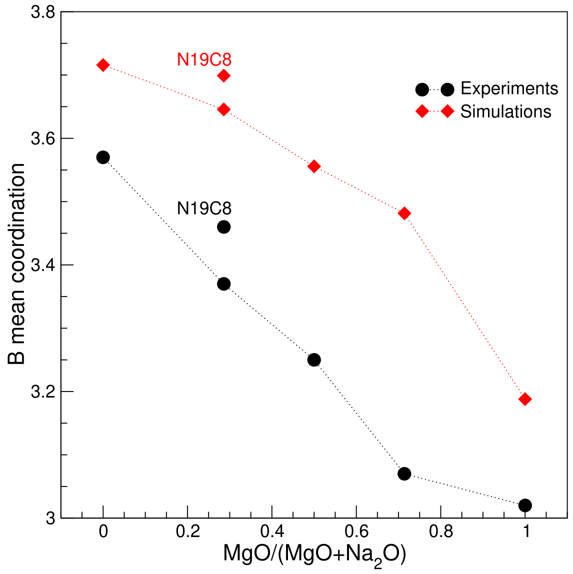

**Figure 6.** Experimental[38] vs calculated B coordination for all glasses. Uncertainties on NMR values are ±1%.

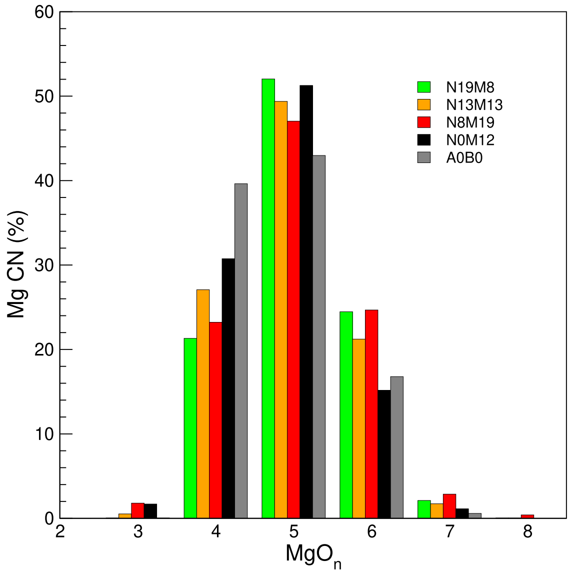

**Figure 7.** Mg coordination distribution of the relevant glasses.

decrease in the average CN for the magnesium-containing glass. A more noticeable decrease is obtained when the magnesium content increases in the series as one has $n_{NaO}$ = 7.85 and 7.21 for N26M0 and N8M19, respectively (Table 3). This indicates that the presence of magnesium impacts alkali coordinations and modifies the environment of sodium in the glasses. A similar analysis indicates that the calcium CN is about 7.39 which is significantly higher than the values found for magnesium.

Finally, no clear trend is found for the magnesium average coordination. A slight decrease is observed between N19M8 and N13M13 while a slight increase between N13M13 and N8M19. Magnesium coordination decreases in the sodium-free glass to $n_{MgO}$ = 4.83, and the simple ternary A0B0 glass displays the lowest value of 4.78, which is close to the one observed for the sodium-free glass, suggesting a possible similar environment. Thus, the distribution of Mg coordination is analyzed in more detail and presented in Figure 7. A small population of under- and over-coordinated ($Mg^{III}$ and $Mg^{VII/VIII}$, respectively) is obtained, which might be artefacts of the potentials used and also depend on the cutoff value (here, $r_{Mg}$ = 2.7 Å). A decrease in penta-coordinated magnesium is obtained with increasing magnesium content in the series, from 52 to 47% $Mg^{V}$ for N19M8 and N8M19, respectively. This decrease mainly promotes the formation of tetra- and hexa-coordinated magnesium, but no clear tendency is observed regarding the preferential formation of one or the other. The simple ternary glass A0B0 displays close proportions of tetra- and penta-coordinated magnesium, with less than 20% of hexa-coordinated units. On the other hand, the sodium-free glass displays similar amount of hexa-coordinated units but significantly higher penta-coordinated magnesium. Beyond the details, the data sets confirm the overall presence of at least three types of magnesium coordination (four-, five-, and six-fold, Figure 7) in the glass series, as suggested by NMR results.[38]

*3.2.2. Bond Angles.* The bond angle distribution (BAD) of several angles of interest are displayed in Figure 8, with mean angle values given in Table 4. The O−Si−O angle is close to 109.5° for all the glasses in the series, in agreement with the tetrahedral geometry of silicon units. In a similar manner, O−Al−O values are around 109° for all glasses, with only minor differences resulting from a slightly increased distortion. The contributions arising for three- and four-fold coordinated boron are clearly evidenced in the O−B−O BAD (Figure 8c) with peaks at around 120 and 109.5°, respectively. The evolution of the intensity of these peaks is consistent with the increasing tri-coordinated boron fraction with increasing magnesium content (Figure 6). The Si−O−Si mean angle value appears to increase overall with increasing magnesium content, which is consistent with a recent Raman spectroscopy result,[38] increasing from 147.2 to 149.1°. Due to the small amount of Al (≃7%), Si−O−Al BADs are quite noisy, which makes the extraction of conclusive information difficult, although a global reduction of the average angle with respect

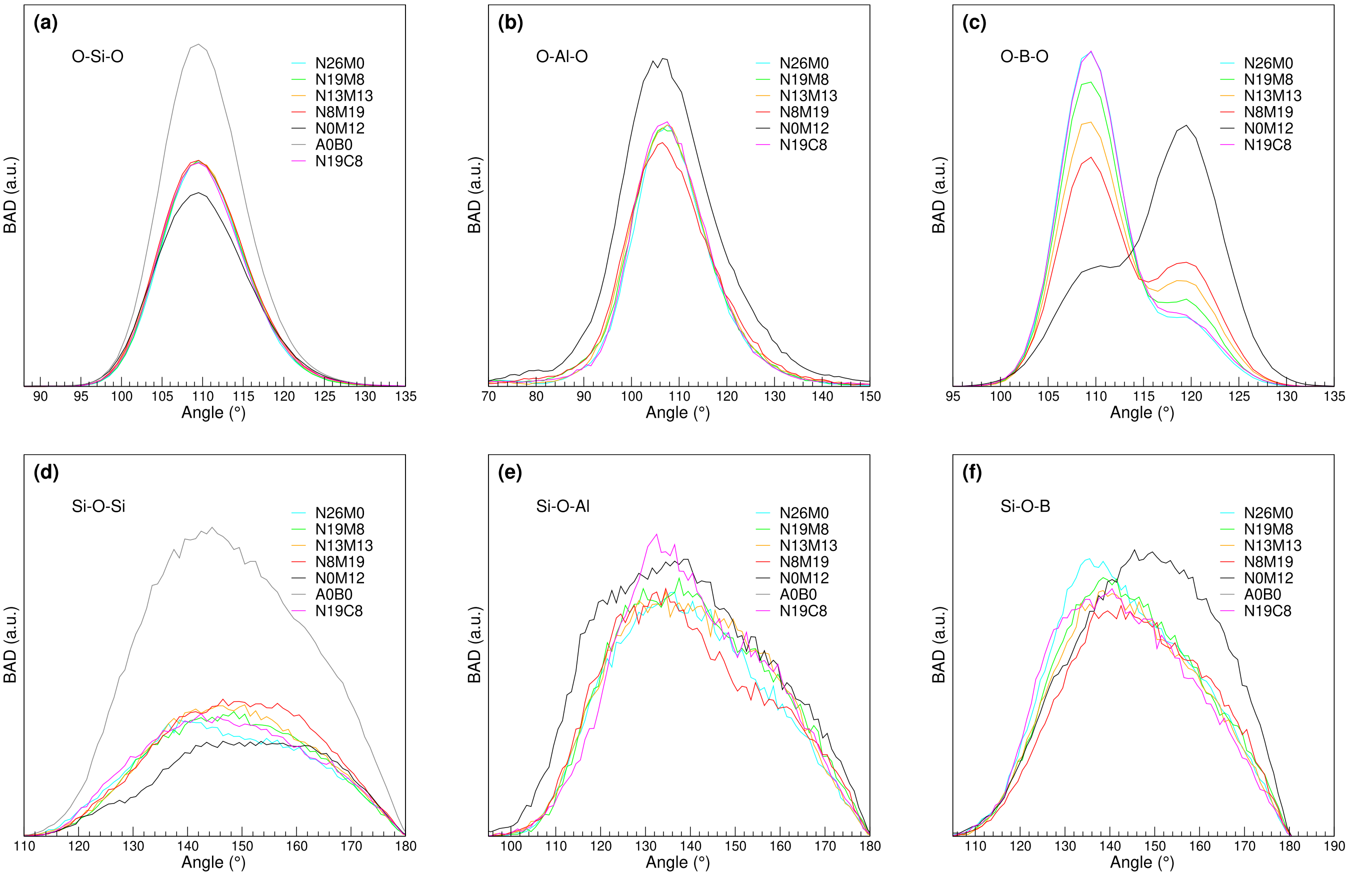

**Figure 8.** BAD for all the glasses.

**Table 4. Simulated Average Angles for All Considered Glasses**

| angle (deg) | N26M0 | N19M8 | N13M13 | N8M19 | N0M12 | A0B0 | N19C8 |
|---|---|---|---|---|---|---|---|
| O−Si−O | 109.4 | 109.4 | 109.4 | 109.4 | 109.4 | 109.4 | 109.4 |
| O−Al−O | 108.9 | 108.9 | 109.0 | 108.9 | 108.9 |  | 109.0 |
| O−B$^{III}$−O | 119.7 | 119.7 | 119.8 | 119.8 | 119.8 |  | 119.8 |
| O−B$^{IV}$−O | 109.4 | 109.4 | 109.4 | 109.4 | 109.4 |  | 109.43 |
| Si−O−Si | 147.2 | 148.2 | 148.2 | 149.1 | 150.4 | 147.4 | 147.3 |
| Si−O−Al | 139.9 | 140.8 | 140.4 | 139.6 | 138.5 |  | 140.7 |
| Si−O−B | 143.7 | 144.8 | 144.5 | 146.2 | 147.8 |  | 143.3 |

**Table 5. CNs of Each Cation−Modifier Pair Associated to Their Respective Cutoff Values**[a]

|  | B−Na | B−Mg\Ca | Al−Na | Al−Mg\Ca | Mg\Ca−Na |  |  |  |  |
|---|---|---|---|---|---|---|---|---|---|
| cutoff (Å) | 4.5 | 3.9/4.1 | 4.7 | 4.1/4.5 | 4.8/4.8 | $R^{\text{Al}}_{\text{Ca/Na}}$ | $R^{\text{Al}}_{\text{Mg/Na}}$ | $R^{\text{B}}_{\text{Ca/Na}}$ | $R^{\text{B}}_{\text{Mg/Na}}$ |
| N26M0 | 4.78 |  | 5.01 |  |  |  |  |  |  |
| N19M8 | 3.30 | 0.62 | 3.83 | 0.61 | 3.21 |  | 1.26 |  | 1.07 |
| N13M13 | 2.33 | 0.99 | 2.98 | 1.06 | 2.16 |  | 1.40 |  | 1.17 |
| N8M19 | 1.37 | 1.50 | 1.90 | 1.67 | 1.34 |  | 1.39 |  | 1.11 |
| N0M12 |  | 0.80 |  | 0.98 |  |  |  |  |  |
| A0B0 |  |  |  |  | 5.13 |  |  |  |  |
| N19C8 | 3.40 | 0.78 | 3.78 | 0.85 | 1.85 | 0.89 |  | 0.87 |  |

[a] Backslash (\) denotes Mg or Ca when applicable. $R^{\text{Former}}_{\text{alkaline-earth/alkali}}$ is the concentration-normalized NCN. Values above one indicates a preferential charge-compensation for the former by the alkali-earth.

to Si−O−Si can be acknowledged. Conversely, the Si−O−B BAD displays significant variations of the mean angle values with increasing Mg content in the glass and is obviously linked to the increase in tri-coordinated boron.

*3.2.3. Preferential Distribution.* Apart from the distribution of cations with oxygen atoms, the spatial distribution of certain cation−cation pairs gives additional insights into the structure of glasses that may not be accessible by other techniques. The environments of B and Al are investigated to obtain an overview of the charge-compensation affinity between Na and Mg (or Ca). Furthermore, the spatial proximity between Na and Mg (or Ca) is investigated to compare the effect of the

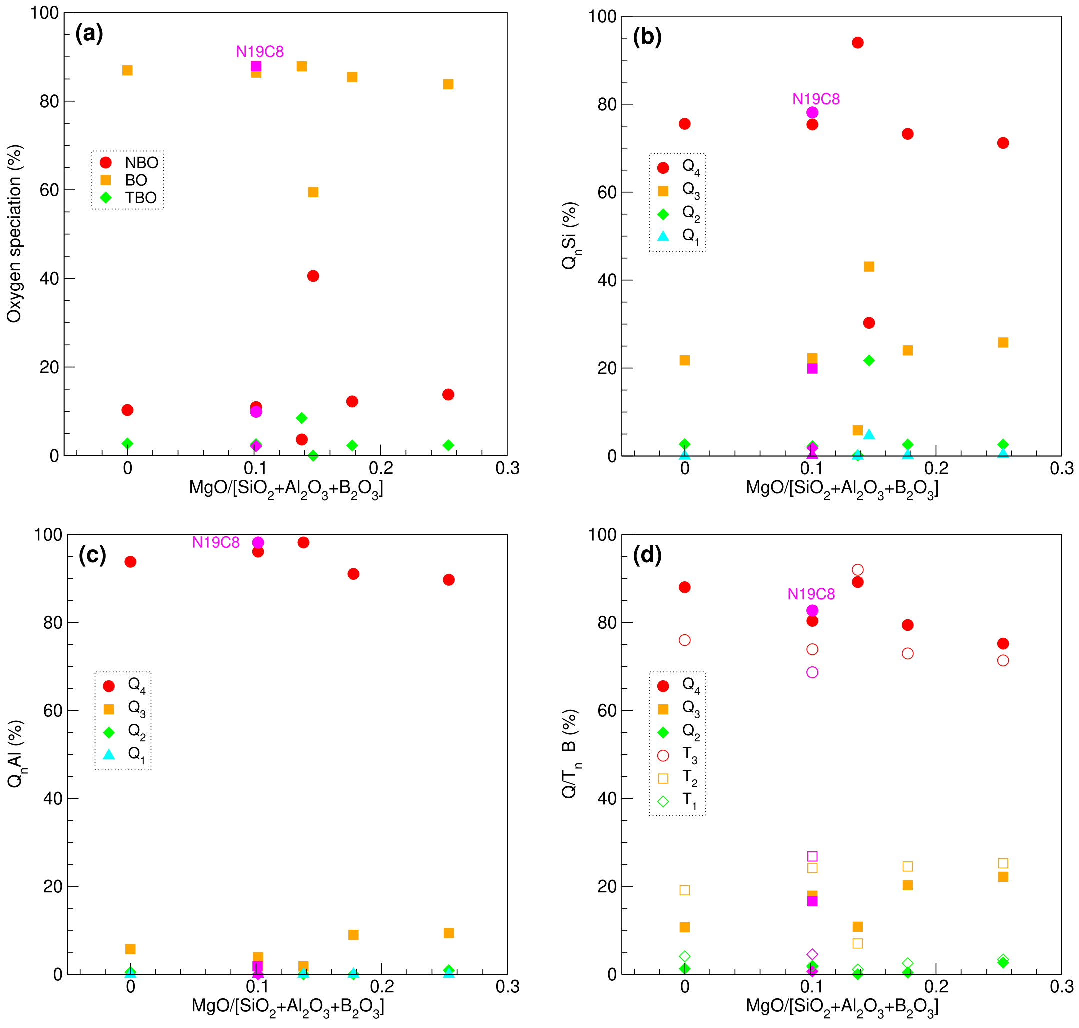

**Figure 9.** Oxygen speciation of all glasses, alongside associated $Q_n$ species for Si, Al, and B. Values are given in the Supporting Information.

two alkaline-earth metals on the sodium environment. The results are listed in Table 5, and those extracted from the partial PDF are displayed in Figure S2 in the Supporting Information.

First, we obtain a B–Na and Al–Na coordination decrease with increasing magnesium content, which is a direct effect of the substitution of Mg with Na. However, when normalized to the quantity of Na present, we observe roughly the same value for both. Nevertheless, when comparing Mg–Na and Ca–Na for N19M8 and N19C8, a significant increase in the number of Na in the vicinity of Mg is observed compared to Ca, by a factor of 1.8. Ca–Na and Mg–Na mixing sites, which can be defined regarding $^{17}$O NMR as a site involving cations interacting with the same NBO (respectively BO) have been observed by NMR,[38,95−97] and a stronger mixing effect of Mg compared to Ca has been suggested in our previous study.[38] While it may not be quantitatively accurate, MD simulations lead to the same trend as observed experimentally. Due to variable Na, Mg, and Ca contents in the studied glasses, the preferential distribution ratio ($R$) of modifier cations around network formers needed to be concentration-normalized (here, called NCN, normalized coordination number). As such, we calculated $R$ from eq 6 (with Ca for N19C8) described elsewhere[70,98]

$$R_{\text{Mg/Na}}^{\text{Former}} = \frac{\text{NCN}_{\text{Former-Mg}}/N_{\text{Mg}}}{\text{NCN}_{\text{Former-Na}}/N_{\text{Na}}} \qquad (6)$$

The results from the calculations are listed in Table 5. A value of $R > 1$ indicates that the alkali-earth cations are preferentially in the vicinity of the network formers. Inversely, if $R < 1$, sodium atoms are preferentially found around network formers. While for the calcium-containing glass, there is a slight preference for network formers to be surrounded by sodium atoms instead of calcium, and the opposite phenomenon occurred for magnesium-containing glasses. Aluminum atoms display a strong preference for magnesium, regardless of the proportion of the latter in the glasses. This preference is even sharper for N13M13 and N8M19, with 40% more presence than sodium. This result seems in opposition with NMR experimental data obtained previously, for which aluminum atoms were preferentially charge-compensated by sodium. However, this preferential distribution does not necessarily reflect preferential charge compensation, as other factors such as the preference of a cation for NBOs might alter this spatial distribution, which will be discussed further in the following section. Usually, in aluminoborosilicates, sodium preferentially compensates for aluminum,[99,100] as compared to calcium or magnesium. Furthermore, in the previous study, we observed that magnesium did not charge-compensate for tetrahedral

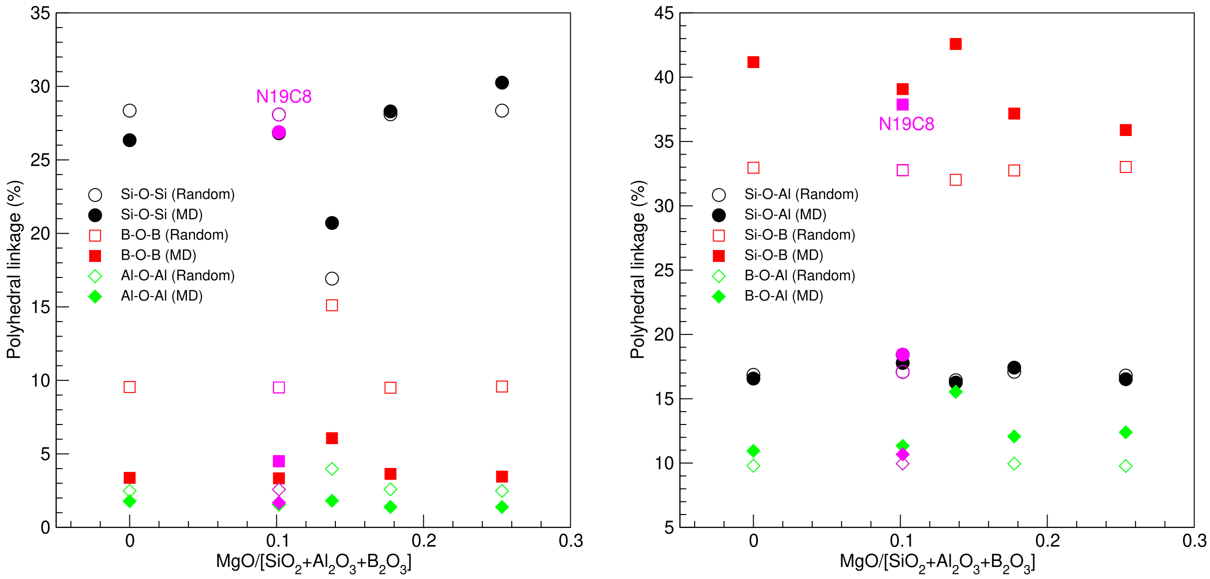

**Figure 10.** Polyhedral linkage of Si−O−Si, B−O−B, and Al−O−Al (left) and Si−O−Al, Si−O−B, and B−O−Al (right) for all the glasses. The calcium-containing glass N19C8 is labeled in magenta.

aluminum units, displaying limited charge-compensating capabilities even when no sodium was available in the glass (N0M12). This may explain why no increase in penta- and hexa-coordinated aluminum in the simulated glass was observed. In a similar manner, magnesium atoms are preferentially found around boron atoms in the simulations, despite displaying the weakest effect as compared to aluminum. Likewise to what was observed for aluminum, boron atoms are compensated by sodium in the experiments, with close to no compensation by magnesium. Indeed, magnesium not only is unable to charge-compensate properly for boron, as detected for N0M12, but also prevents sodium from compensating for boron by generating Mg−Na mixing sites in NBO-rich regions.

*3.2.4. Oxygen Speciation and $Q_n$ Distribution.* The network connectivity can be characterized by quantifying the population of NBO in the glasses, as well as the preferential species bearing them. The so-called $Q_n$ functions can be used, and these are defined by $n$, the number of bridging oxygens (BOs) on an atom. Additionally, the number of tri-bridging oxygens (TBOs) was evaluated for two distinct reasons: (I) their presence in glasses, while not observed directly from experiments nor exactly quantified, has been suggested multiple times to be less than a few percent and (II) a high number of TBOs might suggest artifacts resulting from spurious effects of the potentials. The evolution of BO, NBO and TBO percentages is displayed in Figure 9, together with the silicon, aluminum, and boron $Q_n$ distribution in all glasses (values are given in the Supporting Information).

The number of NBOs is well reproduced by the simulations (Figure 9a), and the calculated values are close to those determined previously.[38] However, while the number of TBOs is below 1−2% in most glasses, N0M12 exhibits up to 8%. This is probably an artifact of the potentials, generating a TBO to compensate for either tetrahedral aluminum or boron units, which explains the discrepancies between the CN of both boron and aluminum obtained from NMR[38] and the simulated ones. As expected from both sodium and magnesium contents, the simple ternary glass A0B0 $Q_4$ population decreases dramatically and promotes both $Q_3$ and $Q_2$ species (Figure 9b). When the magnesium content increased in the series, the number of $Q_4$ species decreases nearly linearly with the ratio of Mg/($SiO_2$ + $Al_2O_3$ + $B_2O_3$), and an increase in $Q_3$ species and a small increase in $Q_2$ is acknowledged. This trend is followed by both silicon and boron, with the latter displaying a similar increase in less polymerized units (mostly $Q_3$ and $T_2$) at the expense of more polymerized $Q_4$ and $T_3$ species. This is consistent with the observed increase in NBOs. It is important to notice that when comparing the evolution of $Q_n$ species for silicon and aluminum, it appears that NBOs exhibit a strong preference for silicon, with only a few percent detected for aluminum (Figure 9c). Investigating further on the percentage of NBO per network former shows indeed a preference for Si units, decreasing with increasing magnesium content, coupled to an increase in preference for B, mainly $B^{III}$ units. Finally, computing the percentage of NBO coordinated by each modifier shows that the NBO coordination of Mg is about twice that of Na (38−45% for Mg and 19−23% for Na). Additionally, when Mg is replaced by Ca, the latter is in the same proportion around NBOs compared to Na, hence almost half as Mg. Normalizing the data by the number of each atom highlights this result in an increased fashion (see Supporting Information Tables S1 and S2). The need to compensate the double positive charge of Mg, coupled with its small radius, is likely to make it more suitable for NBO coordination, as observed experimentally in other systems by Allwardt and Stebbins.[101] However, despite the observed trends, the phase separation observed by NMR between a$Q_4$- and $Q_2$-rich regions[38] is reproduced neither for N8M19 nor for N0M12.

While there is a clear preference of NBOs for silicon units, it is important to notice that there is still a relatively high proportion of NBOs connected to aluminum and boron atoms, distributed between $B^{III}$ and $B^{IV}$. This is in opposition to experimental results for which no NBOs were found around aluminum or boron. For the latter, while NBOs can be expected for some $B^{III}$ units, and there is no evidence of $B^{IV}$ connected to NBOs in the previous study.[38] This can be at the origin of the preferential distribution of Mg around B and Al, as the Mg−O bond is relatively short and Mg atoms are more keen to be found near NBOs, indirectly favoring their presence around network formers while sodium atoms mainly coordinate BOs.

*3.2.5. Polyhedral Linkage.* The linkage between the network forming cations was probed in all the glasses and compared to their counterparts obtained in the case of a statistically random distribution (see Figure 10). Therein, the random distribution[102] was calculated using eqs 7 and 8 with $nO_2$ the number of oxygen atoms as two and only two neighboring network formers, $nF_1$ and $nF_2$ being the number of type one (and two) network former (i.e. Si, B, or Al), and $nF$ the total number of network forming atoms. Equation 8 was used when $F_1$ was different from $F_2$.

$$nO_2 = \frac{nF_1(nF_1 - 1)}{nF(nF - 1)} \tag{7}$$

$$nO_2 = \frac{2 \times nF_1 nF_2}{nF(nF - 1)} \tag{8}$$

The Si−O−Si MD linkage remains overall within values of the random distribution calculation, with no distinction being made for the latter between N19C8 and N19M8. MD simulation results reveal that an increase in the magnesium content increases the Si−O−Si linkage. Both B−O−B and Al−O−Al are found to be significantly lower in MD than expected from a random distribution, roughly by a factor of 2. This confirms the Al avoidance principle in our glass, known as the Loewenstein exclusion.[103] No clear trend was evidenced with Mg content regarding B−O−B linkage, while substituting magnesium for calcium slightly increases (1%) the percentage of B−O−B. On the other hand, Al−O−Al avoidance displays a subtle increase with increasing magnesium content. In a similar way to Si−O−Si, the Si−O−Al MD linkage values are rather close to what is expected from a random distribution. B−O−Al MD linkage values are found to be slightly higher than for the random distribution, but the most salient effect is observed for Si−O−B connectivity, with a 6% decrease with increasing magnesium content.

*3.2.6. Rings.* The ring size distribution in glasses can give further insights into the polymerization degree and overall connectivity of the network. The obtained results are displayed in Figure 11, with mean ring sizes (MRSs) listed in Table 6.

In agreement with the increase in lower $Q_n$ species, A0B0 exhibits the highest ring size distribution of all glasses, with a MRS of above 9. Except for this glass, the MRS of all other structures is centered around 7, in agreement with other studies of glassy systems.[51,104,105] N26M0 and N19C8 display a nearly identical behavior. Increasing magnesium content in the series results in a progressive broadening of the distribution, in agreement with the $Q_n$ evolution and the calculated MRS.

## 4. DISCUSSION

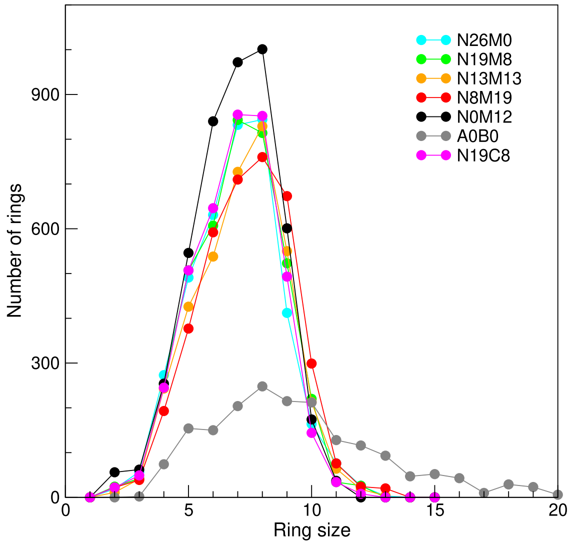

**Figure 11.** Calculated ring size distribution for all the glasses.

**4.1. Accuracy of the Simulated Systems.** We note that the cation−oxygen distance is in good agreement with other studies, and the CN of various species is qualitatively reproduced well. While the aluminum CN is slightly overestimated, the coordination remains mainly around four, as observed by NMR.[38] However, the potentials fail to reproduce the most extreme behavior observed in the sodium-free glass, for which the presence of penta- and hexacoordinated aluminum is observed. MD seems to favor the formation of TBOs to ensure the global charge balance at the expense of the experimentally observed high Al coordination states. It nonetheless appears that the potential for magnesium induced with a same cut-off value overcoordinated more aluminum compared to calcium.

The impact of MgO substitution for both $Na_2O$ and CaO on the boron coordination was reproduced with a great accuracy for such simple potentials: despite being overestimated, the trend of decreasing boron CN with increasing MgO substitution for $Na_2O$ or CaO as compared to experimental findings is reproduced well. This may be for several reasons: when comparing the Mg−Na and Ca−Na environments, it appears that magnesium "attracts" more sodium atoms in its close vicinity, leading to the formation of Mg−Na mixing sites as compared to calcium and as also observed experimentally by NMR.[38] Conversely, preferential distribution analysis reveals that the MD simulations favor $B^{IV}$ proximity of magnesium instead of sodium, which may be to some extent linked to charge compensation. The preferential charge compensation mechanism is in disagreement with experimental results,[10,13,38] which reveals the magnesium's poor charge-compensating capabilities regarding boron, and, to some extent, aluminum. Regarding the latter, magnesium is preferentially found around aluminum in the simulations which are barely observed experimentally.

This discrepancy can be explained (indirectly) by the stronger affinity of Mg for NBOs compared to sodium (see Supporting Information Table S2) as follows (note that the number of NBO given by MD is nearly identical to calculations based on experiments). A deeper analysis of the MD simulations (see the Supporting Information) revealed a wide and non-selective distribution of the NBO on various network-former units: as expected, tetrahedral silicon units, but also a non-negligible fraction of spurious Al−NBO, $B^{IV}$−NBO, and to some extent $B^{III}$−NBO contribution. As a result, magnesium atoms, with a small radius and strong affinity for NBO, are often found in the close vicinity of aluminum and boron atoms. As a secondary effect, NBOs on $B^{IV}$ and $Al^{IV}$ are unlikely to form based on our previous $^{17}O$ NMR data,[38] which may result in the discrepancies observed in MD. This severely impacted the N0M12 glass where $Al^{V}$ and $Al^{VI}$ are in insufficient proportions compared to $^{27}Al$ NMR experiments.[38] Further discussion on these effect requires a deeper analysis of

**Table 6. MRS of Different Glasses**

| | N26M0 | N19M8 | N13M13 | N8M19 | N0M12 | A0B0 | N19C8 |
|---|---|---|---|---|---|---|---|
| MRS | 6.96 | 7.03 | 7.16 | 7.36 | 6.92 | 9.32 | 6.93 |

the $^{17}$O NMR data based on the DFT computation from MD.[106] This work is in progress and will be presented elsewhere.

The BAD results are consistent with trends observed by Raman spectroscopy regarding Si−O−Si aperture with increasing magnesium content and, to some extent, with the increased distortion of aluminum tetrahedra with increasing magnesium content. However, more subtle effects are not realistically reproduced such as the increasing polymerization degree with increasing magnesium content up to a separation into two sub-networks. The cation−oxygen environment is effectively reproduced, but there might be a lack of refined cation−cation interactions, which results in some of the observed discrepancies between simulations and experimental results. Additionally, Al/Si/B mixing might not be effectively reproduced, as there is no clear increase of B−O−B contribution, for instance, which has been observed experimentally.[38] The development of parameters regarding these interactions, either through machine learning or the use of polarizable terms, for instance, might significantly improve the numerical description of these glasses, the present simulations representing an interesting benchmark for such alternative numerical schemes.

Hence, the simulated vitreous systems overall appear to be reproduced well, which supports the claimed transferability of the potentials to more complex systems.[41] This allows further analysis of the structure as well as a strong basis for structure−composition−property relationships.

### 4.2. Magnesium Environment and Medium-Range Order.

The magnesium environment has been difficult to determine experimentally by NMR[38] due to several factors, namely, the broad distribution of its environment, its high quadrupolar interactions, and the lack of data available in the literature. MD may, therefore, provide some insights into the local environment of magnesium in the studied glasses and how it affects the medium-range order. Compared to experiments, the distribution of the magnesium environment by MD can be precisely evaluated, provided that the vitreous systems are accurately reproduced. As such, and considering the degree of accuracy of the simulations, some trends can be observed. Based on NMR spectroscopy, it was suggested that increasing magnesium content in the series promoted an overall increase in mean coordination from five to six. This trend was not well reproduced by the simulations; the increasing magnesium content seems to induce an increase in both tetra- and hexacoordinated magnesium. This could, however, partly explain the increase in the width of the $^{25}$Mg NMR spectra, but a more accurate analysis will require better potentials or ab-initio calculation, and simulation of NMR spectra might allow one to unravel this matter. Additionally, the direct CN analysis, as displayed in Figure 5d, shows a more defined plateau for magnesium than for calcium. While not as well-defined as for network-forming species, this could be indicative of the fact that magnesium behaves to some extent as an intermediate. Keeping these results in mind, two scenarios emerge: (I) magnesium behaved as a network modifier and as such is not considered as part of the rings or (II) magnesium behaves to some extent as an intermediate/network former and impacts the characteristics of MRO (see Figure 12).

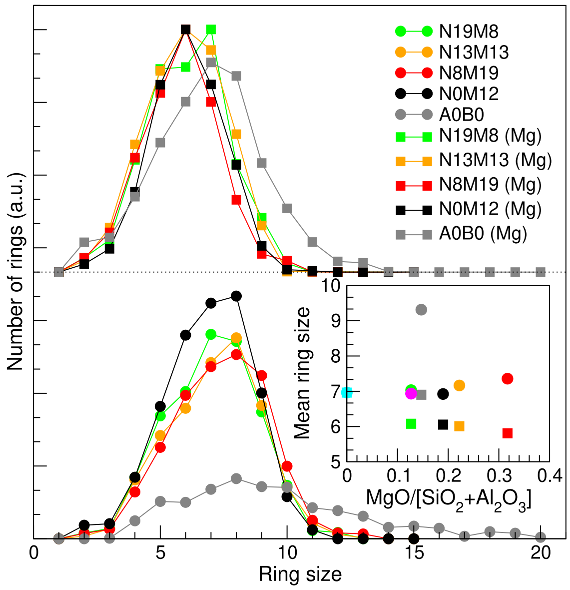

**Figure 12.** Ring size distribution of magnesium-containing glasses with (above, squares) and without (below, circles) considering magnesium as part of the rings. The inset displays the MRS of all glasses in both cases, with their respective symbol shapes.

If magnesium is considered as a modifier, increasing magnesium content in the glass series induces a progressive increase in the MRS, in respect of the depolymerization of the glassy system, as it is observed with the decrease in $Q_4$ (Figure 9) as well as the increase in NBO, as observed by MD and NBO calculations based on experimental data. Additionally, it has been observed that NBOs tend to be found nearly twice more often around Mg than Na or Ca. Conversely, taking magnesium into account as a part of the ring structure drastically changes the observed tendency. The MRS, centered around 7 in the first case, shifts to a mean value centered around 6, coupled to a trend in the decrease of the MRS with increasing magnesium content. Hence, increasing magnesium content in the series resulted in a more polymerized and slightly more ordered network, which can be linked with the overall decrease in the width of the ring size distribution. In that case, the observed trend is more in line with experimental data.

## 5. CONCLUSIONS

Seven three- to-five-oxide silicate glasses have been simulated by classical MD and compared to a set of previously obtained NMR and Raman spectroscopy experimental data[38] as well as new neutron scattering experiments. The set, composed of four magnesium-containing aluminoborosilicate glasses, an additional calcium-containing glass, a sodium aluminoborosilicate glass, and a simple reference silicate glass, allowed for the investigation of the impact of various sodium/magnesium substitutions on the structure of these glasses as well as highlighting the differences between calcium and magnesium environments.

Structural models obtained by numerical simulations are overall in quite good agreement with the experimental data among which the structure functions $g(r)$ and $S(k)$ indicate that the used force field takes into account the complexity of these glassy systems and is able to reproduce some salient features. Various cation−oxygen bond length are also consistent with neutron scattering data but with slight discrepancies mostly arising from sodium-related interactions impacting the MRO. The BAD was accurately reproduced and seemed consistent with the increase of the mean Si−O−Si angle with increasing magnesium content, as observed by Raman spectra.

Short-range features such as cation−oxygen coordination were fairly well reproduced—with the exception of one glass for which the fraction of TBOs is too high and results in mostly four-fold aluminum, the CN of the latter being fairly reproduced. Most importantly, the trend in decreasing tetrahedral boron with increasing magnesium content is qualitatively reproduced well, as well as the observed decrease when calcium is substituted by magnesium. Regarding the latter, while the mean coordination does not seem to follow experimental data which are difficult to resolve, MD allows highlighting a potential separation from penta- to tetra- and hexahedral magnesium in the series, which might explain the broadening of the $^{25}$Mg MAS NMR spectra reported elsewhere.[38] Analysis of the MRO through rings highlights the potential impact of magnesium on the polymerization degree of the glasses.

The overall discrepancies probably arise from spurious preferential charge compensation by magnesium of both aluminum and boron, network formers that were predicted by MD to bond to a too large fraction of NBOs. As a result, magnesium atoms with a higher affinity to NBOs are found in the vicinity of $B^{IV}$ and $Al^{IV}$, more than expected from $^{17}$O experiments. More subtle effects such as the presence of Mg−Na mixing sites could not be really resolved, as it may be the result of the spurious effect considering the lack of refined cation−cation interactions. More refined structure may be achievable through the use of other potential parameters/types, such as polarizable potentials (not available to the best of our knowledge) or the use of reverse Monte Carlo simulations using structural data to constrain the systems. Having these results in hand, the simulated systems offer an interesting basis for further property calculations that could be compared to other experimental findings, while also establishing in a neat way a composition−structure relationship for multicomponent silicates.

## ■ ASSOCIATED CONTENT

### Supporting Information

The Supporting Information is available free of charge at https://pubs.acs.org/doi/10.1021/acs.jpcb.1c06990.

> All calculated partial structure factors, cation−cation PDFs, values of NBOs per network former and their preference, NBOs per network modifiers and their preference, and $Q_n$ for Si, Al, and B for different glasses (PDF)

## ■ AUTHOR INFORMATION

### Corresponding Authors

**M. Micoulaut** − *Sorbonne Université, Laboratoire de Physique Théorique de la Matière Condensée, CNRS UMR 7600, 75252 Paris Cedex 05, France*; Email: matthieu.micoulaut@sorbonne-universite.fr

**J.-M. Delaye** − *CEA, DES, ISEC, DE2D, Université de Montpellier, 30207 Bagnols-sur-Cèze Cedex, France*; Email: jean-marc.delaye@cea.fr

### Authors

**N. Bisbrouck** − *CEA, DES, ISEC, DE2D, Université de Montpellier, 30207 Bagnols-sur-Cèze Cedex, France*; orcid.org/0000-0003-1903-3032

**M. Bertani** − *Université Paris-Saclay, CEA, CNRS, NIMBE, 91191 Gif-sur-Yvette, France; Department of Chemical and Geological Sciences, University of Modena and Reggio Emilia, 41125 Modena, Italy*

**T. Charpentier** − *Université Paris-Saclay, CEA, CNRS, NIMBE, 91191 Gif-sur-Yvette, France*; orcid.org/0000-0002-3034-1389

**S. Gin** − *CEA, DES, ISEC, DE2D, Université de Montpellier, 30207 Bagnols-sur-Cèze Cedex, France*; orcid.org/0000-0002-1950-9195

**F. Angeli** − *CEA, DES, ISEC, DE2D, Université de Montpellier, 30207 Bagnols-sur-Cèze Cedex, France*

Complete contact information is available at: https://pubs.acs.org/10.1021/acs.jpcb.1c06990

### Notes

The authors declare no competing financial interest.

## ■ ACKNOWLEDGMENTS

This study was supported by the French Alternative Energies and Atomic Energy Commission (CEA) and Electricité de France (EDF).

## ■ REFERENCES

(1) Arnett, D. Supernovae and Nucleosynthesis: An Investigation of the History of Matter from the Big Bang to the Present. In *Supernovae and Nucleosynthesis: An Investigation of the History of Matter, from the Big Bang to the Present*; Arnett, D., Ed.; Princeton University Press: Princeton, 1996; Vol. *1996*.

(2) Rudnick, R. L.; Gao, S. Composition of the Continental Crust. In *Treatise on Geochemistry*; Holland, H. D., Turekian, K. K., Eds.; Pergamon: Oxford, 2003; pp 1−64.

(3) Taylor, S. R.; McLennan, S. M. *The Continental Crust: Its Composition and Evolution*; Blackwell Scientific Publishing, 1985.

(4) Karki, B. B.; Stixrude, L. P. Viscosity of MgSiO3 Liquid at Earth's Mantle Conditions: Implications for an Early Magma Ocean. *Science* **2010**, *328*, 740.

(5) Stixrude, L.; Karki, B. Structure and Freezing of MgSiO 3 Liquid in Earth's Lower Mantle. *Science* **2005**, *310*, 297.

(6) Urbain, G.; Bottinga, Y.; Richet, P. Viscosity of liquid silica, silicates and alumino-silicates. *Geochim. Cosmochim. Acta* **1982**, *46*, 1061−1072.

(7) Morse, D. L.; Evenson, J. W. Welcome to the Glass Age. *Int. J. Appl. Glass Sci.* **2016**, *7*, 409−412.

(8) Smedskjaer, M. M.; Youngman, R. E.; Mauro, J. C. Principles of Pyrex glass chemistry: structure-property relationships. *Appl. Phys. A: Mater. Sci. Process.* **2014**, *116*, 491−504.

(9) Ball, P. Concrete mixing for gorillas. *Nat. Mater.* **2015**, *14*, 472.

(10) Backhouse, D. J.; Corkhill, C. L.; Hyatt, N. C.; Hand, R. J. Investigation of the role of Mg and Ca in the structure and durability of aluminoborosilicate glass. *J. Non-Cryst. Solids* **2019**, *512*, 41−52.

(11) Thien, B. M. J.; Godon, N.; Ballestero, A.; Gin, S.; Ayral, A. The dual effect of Mg on the long-term alteration rate of AVM nuclear waste glasses. *J. Nucl. Mater.* **2012**, *427*, 297−310.

(12) Vernaz, É.; Bruezière, J. History of Nuclear Waste Glass in France. *Procedia Mater. Sci.* **2014**, *7*, 3−9.

(13) Guo, R.; Brigden, C. T.; Gin, S.; Swanton, S. W.; Farnan, I. The effect of magnesium on the local structure and initial dissolution rate of simplified UK Magnox waste glasses. *J. Non-Cryst. Solids* **2018**, *497*, 82−92.

(14) Harrison, M. T. The Effect of Composition on Short- and Long-term Durability of UK HLW Glass. *Procedia Mater. Sci.* **2014**, *7*, 186−192.

(15) Oliveira, J. M.; Correia, R. N.; Fernandes, M. H.; Rocha, J. Influence of the CaO/MgO ratio on the structure of phase-separated glasses: a solid state 29Si and 31P MAS NMR study. *J. Non-Cryst. Solids* **2000**, *265*, 221−229.

(16) Kokubo, T.; Kushitani, H.; Ohtsuki, C.; Sakka, S.; Yamamuro, T. Chemical reaction of bioactive glass and glass-ceramics with a simulated body fluid. *J. Mater. Sci.: Mater. Med.* **1992**, *3*, 79−83.

(17) Diba, M.; Tapia, F.; Boccaccini, A. R.; Strobel, L. A. Magnesium-Containing Bioactive Glasses for Biomedical Applications. *Int. J. Appl. Glass Sci.* **2012**, *3*, 221−253.

(18) Bellucci, D.; Veronesi, E.; Dominici, M.; Cannillo, V. A new bioactive glass with extremely high crystallization temperature and outstanding biological performance. *Mater. Sci. Eng., C* **2020**, *110*, 110699.

(19) Bechgaard, T. K.; Scannell, G.; Huang, L.; Youngman, R. E.; Mauro, J. C.; Smedskjaer, M. M. Structure of MgO/CaO sodium aluminosilicate glasses: Raman spectroscopy study. *J. Non-Cryst. Solids* **2017**, *470*, 145−151.

(20) Bradtmüller, H.; Uesbeck, T.; Eckert, H.; Murata, T.; Nakane, S.; Yamazaki, H. Structural Origins of Crack Resistance on Magnesium Aluminoborosilicate Glasses Studied by Solid-State NMR. *J. Phys. Chem. C* **2019**, *123*, 14941−14954.

(21) Mauro, J. C.; Tandia, A.; Vargheese, K. D.; Mauro, Y. Z.; Smedskjaer, M. M. Accelerating the Design of Functional Glasses through Modeling. *Chem. Mater.* **2016**, *28*, 4267−4277.

(22) Wang, M.; Smedskjaer, M.; Mauro, J.; Sant, G.; Bauchy, M. Topological Origin of the Network Dilation Anomaly in Ion-Exchanged Glasses. *Phys. Rev. Appl.* **2017**, *8*, 054040.

(23) Logrado, M.; Eckert, H.; Murata, T.; Nakane, S.; Yamazaki, H. Structure-property relations in crack-resistant alkaline-earth aluminoborosilicate glasses studied by solid state NMR. *J. Am. Ceram. Soc.* **2021**, *104*, 2250. WOS:000610789200001

(24) Gin, S.; Beaudoux, X.; Angéli, F.; Jégou, C.; Godon, N. Effect of composition on the short-term and long-term dissolution rates of ten borosilicate glasses of increasing complexity from 3 to 30 oxides. *J. Non-Cryst. Solids* **2012**, *358*, 2559−2570.

(25) Guignard, M.; Cormier, L. Environments of Mg and Al in MgO-Al2O3-SiO2 glasses: A study coupling neutron and X-ray diffraction and Reverse Monte Carlo modeling. *Chem. Geol.* **2008**, *256*, 111−118.

(26) Cormier, L.; Cuello, G. J. Structural investigation of glasses along the MgSiO3-CaSiO3 join: Diffraction studies. *Geochim. Cosmochim. Acta* **2013**, *122*, 498−510.

(27) Pedone, A.; Malavasi, G.; Menziani, M. C.; Segre, U.; Cormack, A. N. Role of magnesium in soda-lime glasses: insight into structural, transport, and mechanical properties through computer simulations. *J. Phys. Chem. C* **2008**, *112*, 11034−11041.

(28) Wilding, M. C.; Benmore, C. J.; Tangeman, J. A.; Sampath, S. Evidence of different structures in magnesium silicate liquids: coordination changes in forsterite- to enstatite-composition glasses. *Chem. Geol.* **2004**, *213*, 281−291.

(29) Trcera, N. *Etude de la Structure de Verres Magnésio-Silicatés : Approche Expérimentale et Modélisation. Phdthesis*; Université Paris-Est, 2008.

(30) Morizet, Y.; Trcera, N.; Larre, C.; Rivoal, M.; Le Menn, E.; Vantelon, D.; Gaillard, F. X-ray absorption spectroscopic investigation of the Ca and Mg environments in CO2-bearing silicate glasses. *Chem. Geol.* **2019**, *510*, 91−102.

(31) Neuville, D. R.; Cormier, L.; Montouillout, V.; Florian, P.; Millot, F.; Rifflet, J.-C.; Massiot, D. Amorphous materials: Properties, structure, and durability: Structure of Mg- and Mg/Ca aluminosilicate glasses: 27Al NMR and Raman spectroscopy investigations. *Am. Mineral.* **2008**, *93*, 1721−1731.

(32) Trcera, N.; Rossano, S.; Tarrida, M. Structural study of Mg-bearing sodosilicate glasses by Raman spectroscopy. *J. Raman Spectrosc.* **2011**, *42*, 765−772.

(33) Maekawa, H.; Maekawa, T.; Kawamura, K.; Yokokawa, T. The structural groups of alkali silicate glasses determined from 29Si MAS-NMR. *J. Non-Cryst. Solids* **1991**, *127*, 53−64.

(34) Shimoda, K.; Nemoto, T.; Saito, K. Local Structure of Magnesium in Silicate Glasses: A 25Mg 3QMAS NMR Study. *J. Phys. Chem. B* **2008**, *112*, 6747−6752.

(35) Shimoda, K.; Tobu, Y.; Hatakeyama, M.; Nemoto, T.; Saito, K. Structural investigation of Mg local environments in silicate glasses by ultra-high field 25Mg 3QMAS NMR spectroscopy. *Am. Mineral.* **2007**, *92*, 695−698.

(36) Freitas, J. C. C.; Smith, M. E. Recent Advances in Solid-State 25Mg NMR Spectroscopy. In *Annual Reports on NMR Spectroscopy*; Webb, G. A., Ed.; Academic Press, 2012; Vol. 75, pp 25−114.

(37) Kroeker, S.; Stebbins, J. F. Magnesium coordination environments in glasses and minerals: New insight from high-field magnesium-25 MAS NMR. *Am. Mineral.* **2000**, *85*, 1459−1464.

(38) Bisbrouck, N.; Bertani, M.; Angeli, F.; Charpentier, T.; Ligny, D.; Delaye, J. M.; Gin, S.; Micoulaut, M. Impact of magnesium on the structure of aluminoborosilicate glasses: A solid-state NMR and Raman spectroscopy study. *J. Am. Ceram. Soc.* **2021**, *104*, 4518−4536.

(39) Pedone, A.; Malavasi, G.; Menziani, M. C. Computational Insight into the Effect of CaO/MgO Substitution on the Structural Properties of Phospho-Silicate Bioactive Glasses. *J. Phys. Chem. C* **2009**, *113*, 15723−15730.

(40) Du, J.; Cormack, A. N. The medium range structure of sodium silicate glasses: a molecular dynamics simulation. *J. Non-Cryst. Solids* **2004**, *349*, 66−79.

(41) Wang, M.; Anoop Krishnan, N. M.; Wang, B.; Smedskjaer, M. M.; Mauro, J. C.; Bauchy, M. A new transferable interatomic potential for molecular dynamics simulations of borosilicate glasses. *J. Non-Cryst. Solids* **2018**, *498*, 294−304.

(42) Tuheen, M. I.; Deng, L.; Du, J. A comparative study of the effectiveness of empirical potentials for molecular dynamics simulations of borosilicate glasses. *J. Non-Cryst. Solids* **2021**, *553*, 120413.

(43) Angeli, F.; Delaye, J.-M.; Charpentier, T.; Petit, J.-C.; Ghaleb, D.; Faucon, P. Influence of glass chemical composition on the Na-O bond distance: a 23Na 3Q-MAS NMR and molecular dynamics study. *J. Non-Cryst. Solids* **2000**, *276*, 132−144.

(44) Du, J.; Benmore, C. J.; Corrales, R.; Hart, R. T.; Weber, J. K. R. A molecular dynamics simulation interpretation of neutron and x-ray diffraction measurements on single phase Y2O3-Al2O3glasses. *J. Phys.: Condens. Matter* **2009**, *21*, 205102.

(45) Yu, Y.; Wang, M.; Smedskjaer, M. M.; Mauro, J. C.; Sant, G.; Bauchy, M. Thermometer Effect: Origin of the Mixed Alkali Effect in Glass Relaxation. *Phys. Rev. Lett.* **2017**, *119*, 095501.

(46) Wilkinson, C. J.; Potter, A. R.; Welch, R. S.; Bragatto, C.; Zheng, Q.; Bauchy, M.; Affatigato, M.; Feller, S. A.; Mauro, J. C. Topological Origins of the Mixed Alkali Effect in Glass. *J. Phys. Chem. B* **2019**, *123*, 7482−7489.

(47) Lee, K.-H.; Yang, Y.; Ziebarth, B.; Mannstadt, W.; Davis, M. J.; Mauro, J. C. Evaluation of classical interatomic potentials for molecular dynamics simulations of borosilicate glasses. *J. Non-Cryst. Solids* **2020**, *528*, 119736.

(48) Deng, L.; Du, J. Development of boron oxide potentials for computer simulations of multicomponent oxide glasses. *J. Am. Ceram. Soc.* **2019**, *102*, 2482−2505.

(49) Inoue, H.; Masuno, A.; Watanabe, Y. Modeling of the Structure of Sodium Borosilicate Glasses Using Pair Potentials. *J. Phys. Chem. B* **2012**, *116*, 12325−12331.

(50) Kieu, L.-H.; Delaye, J.-M.; Cormier, L.; Stolz, C. Development of empirical potentials for sodium borosilicate glass systems. *J. Non-Cryst. Solids* **2011**, *357*, 3313−3321.

(51) Deng, L.; Du, J. Development of effective empirical potentials for molecular dynamics simulations of the structures and properties of boroaluminosilicate glasses. *J. Non-Cryst. Solids* **2016**, *453*, 177−194.

(52) Sundararaman, S.; Huang, L.; Ispas, S.; Kob, W.; New interaction potentials for borate glasses with mixed network formers, *J. Chem. Phys.*. American Institute of Physics: Publisher, 2020; Vol. *152*, p 104501. DOI: 10.1063/1.5142605

(53) Shih, Y.-T.; Sundararaman, S.; Ispas, S.; Huang, L. New interaction potentials for alkaline earth silicate and borate glasses. *J. Non-Cryst. Solids* **2021**, *565*, 120853.

(54) Plimpton, S. Fast Parallel Algorithms for Short-Range Molecular Dynamics. *J. Comput. Phys.* **1995**, *117*, 1−19.

(55) Guillot, B.; Sator, N. A computer simulation study of natural silicate melts. Part I: Low pressure properties. *Geochim. Cosmochim. Acta* **2007**, *71*, 1249−1265.

(56) Li, X.; Song, W.; Yang, K.; Krishnan, N. M. A.; Wang, B.; Smedskjaer, M. M.; Mauro, J. C.; Sant, G.; Balonis, M.; Bauchy, M. Cooling rate effects in sodium silicate glasses: Bridging the gap between molecular dynamics simulations and experiments. *J. Chem. Phys.* **2017**, *147*, 074501.

(57) Mantisi, B.; Bauchy, M.; Micoulaut, M. Cycling through the glass transition: Evidence for reversibility windows and dynamic anomalies. *Phys. Rev. B* **2015**, *92*, 134201.

(58) Bauchy, M.; Micoulaut, M. Densified network glasses and liquids with thermodynamically reversible and structurally adaptive behaviour. *Nat. Commun.* **2015**, *6*, 6398.

(59) Liu, Z.; Hu, Y.; Li, X.; Song, W.; Goyal, S.; Micoulaut, M.; Bauchy, M. Glass relaxation and hysteresis of the glass transition by molecular dynamics simulations. *Phys. Rev. B* **2018**, *98*, 104205.

(60) Deng, L.; Du, J. Effects of system size and cooling rate on the structure and properties of sodium borosilicate glasses from molecular dynamics simulations. *J. Chem. Phys.* **2018**, *148*, 024504.

(61) Wright, A. C. The comparison of molecular dynamics simulations with diffraction experiments. *J. Non-Cryst. Solids* **1993**, *159*, 264−268.

(62) Sears, V. F. Neutron scattering lengths and cross sections. *Neutron News* **1992**, *3*, 26−37.

(63) Le Roux, S.; Jund, P. Ring statistics analysis of topological networks: New approach and application to amorphous GeS2 and SiO2 systems. *Comput. Mater. Sci.* **2010**, *49*, 70−83.

(64) King, S. V. Ring Configurations in a Random Network Model of Vitreous Silica. *Nature* **1967**, *213*, 1112−1113.

(65) Franzblau, D. S. Computation of ring statistics for network models of solids. *Phys. Rev. B: Condens. Matter Mater. Phys.* **1991**, *44*, 4925−4930.

(66) Cuello, G. J.; Darpentigny, J.; Hennet, L.; Cormier, L.; Dupont, J.; Homatter, B.; Beuneu, B. 7C2, the new neutron diffractometer for liquids and disordered materials at LLB. *J. Phys.: Conf. Ser.* **2016**, *746*, 012020.

(67) Howe, M. A.; McGreevy, R. L.; Zetterström, P. *CORRECT: A Correction Program for Neutron Diffraction Data*; NFL Studsvik Internal Report, 1996.

(68) Keen, D. A. A comparison of various commonly used correlation functions for describing total scattering. *J. Appl. Crystallogr.* **2001**, *34*, 172−177.

(69) Farrow, C. L.; Billinge, S. J. L. Relationship between the atomic pair distribution function and small-angle scattering: implications for modeling of nanoparticles. *Acta Crystallogr., Sect. A: Found. Crystallogr.* **2009**, *65*, 232−239.

(70) Lu, X.; Reiser, J. T.; Parruzot, B.; Deng, L.; Gussev, I. M.; Neuefeind, J. C.; Graham, T. R.; Liu, H.; Ryan, J. V.; Kim, S. H.; Washton, N.; Lang, M.; Du, J.; Vienna, J. D. Effects of Al:Si and (Al + Na):Si ratios on the properties of the international simple glass, part II: Structure. *J. Am. Ceram. Soc.* **2021**, *104*, 183−207.

(71) Sivia, D. S. *Elementary Scattering Theory: For X-ray and Neutron Users*; Oxford University Press, 2011.

(72) Lorch, E. Neutron diffraction by germania, silica and radiation-damaged silica glasses. *J. Phys. C: Solid State Phys.* **1969**, *2*, 229−237.

(73) Gaskell, P. H. Medium-range order and random networks. *J. Non-Cryst. Solids* **2001**, *293−295*, 146−152.

(74) Benmore, C. J.; Hart, R. T.; Mei, Q.; Price, D. L.; Yarger, J.; Tulk, C. A.; Klug, D. D. Intermediate range chemical ordering in amorphous and liquid water, Si, and Ge. *Phys. Rev. B: Condens. Matter Mater. Phys.* **2005**, *72*, 132201.

(75) Micoulaut, M.; Coulet, M.-V.; Piarristeguy, A.; Johnson, M. R.; Cuello, G. J.; Bichara, C.; Raty, J.-Y.; Flores-Ruiz, H.; Pradel, A. Effect of concentration in Ge-Te liquids: A combined density functional and neutron scattering study. *Phys. Rev. B: Condens. Matter Mater. Phys.* **2014**, *89*, 174205.

(76) Micoulaut, M. Diffraction patterns of amorphous materials as a series expansion of neighbor distribution functions. *J. Phys.: Condens. Matter* **2019**, *31*, 285402.

(77) Du, J.; Xiang, Y. Investigating the structure-diffusion-bioactivity relationship of strontium containing bioactive glasses using molecular dynamics based computer simulations. *J. Non-Cryst. Solids* **2016**, *432*, 35−40.

(78) Greaves, G. N.; Fontaine, A.; Lagarde, P.; Raoux, D.; Gurman, S. J. Local structure of silicate glasses. *Nature* **1981**, *293*, 611−616.

(79) Galoisy, L.; Pélegrin, E.; Arrio, M.-A.; Ildefonse, P.; Calas, G.; Ghaleb, D.; Fillet, C.; Pacaud, F. Evidence for 6-Coordinated Zirconium in Inactive Nuclear Waste Glasses. *J. Am. Ceram. Soc.* **1999**, *82*, 2219−2224.

(80) Collin, M.; Fournier, M.; Frugier, P.; Charpentier, T.; Moskura, M.; Deng, L.; Ren, M.; Du, J.; Gin, S. Structure of International Simple Glass and properties of passivating layer formed in circumneutral pH conditions. *npj Mater. Degrad.* **2018**, *2*, 4.

(81) Michel, F.; Cormier, L.; Lombard, P.; Beuneu, B.; Galoisy, L.; Calas, G. Mechanisms of boron coordination change between borosilicate glasses and melts. *J. Non-Cryst. Solids* **2013**, *379*, 169−176.

(82) Majérus, O.; Cormier, L.; Calas, G.; Beuneu, B. Temperature-induced boron coordination change in alkali borate glasses and melts. *Phys. Rev. B: Condens. Matter Mater. Phys.* **2003**, *67*, 024210.

(83) Krogh-Moe, J. The structure of vitreous and liquid boron oxide. *J. Non-Cryst. Solids* **1969**, *1*, 269−284.

(84) Pedesseau, L.; Ispas, S.; Kob, W. First-principles study of a sodium borosilicate glass-former. II. The glass state. *Phys. Rev. B* **2015**, *91*, 134202.

(85) Cormier, L.; Ghaleb, D.; Delaye, J.-M.; Calas, G. Competition for charge compensation in borosilicate glasses: Wide-angle x-ray scattering and molecular dynamics calculations. *Phys. Rev. B: Condens. Matter Mater. Phys.* **2000**, *61*, 14495−14499.

(86) Waseda, Y.; Toguri, J. M. The structure of molten binary silicate systems CaO-SiO2 and MgO-SiO2. *Metall. Trans. B* **1977**, *8*, 563−568.

(87) Taniguchi, T.; Okuno, M.; Matsumoto, T. X-ray diffraction and EXAFS studies of silicate glasses containing Mg, Ca and Ba atoms. *J. Non-Cryst. Solids* **1997**, *211*, 56−63.

(88) Okuno, M.; Marumo, F. The structure analyses of pyrope (Mg3Al2Si3Ol2) and grossular (Ca3Al2Si3O12) glasses by X-ray diffraction method. *Mineral. J.* **1993**, *16*, 407−415.

(89) Eckersley, M. C.; Gaskell, P. H.; Barnes, A. C.; Chieux, P. Structural ordering in a calcium silicate glass. *iNature* **1988**, *335*, 525−527.

(90) Montorsi, M.; Leonelli, C.; Menziani, M. C.; Du, J.; Cormack, A. N. Molecular dynamics study of zirconia containing glasses. *Phys. Chem. Glasses* **2002**, *43*, 137−142.

(91) Yin, C. D.; Okuno, M.; Morikawa, H.; Marumo, F. Structure analysis of MgSiO3 glass. *J. Non-Cryst. Solids* **1983**, *55*, 131−141.

(92) Tabira, Y. Local structure around oxygen atoms in CaMgSi2O6 glass by O K-edge EXELFS. *Mater. Sci. Eng., B* **1996**, *41*, 63−66.

(93) Yun, Y. H.; Bray, P. J. Nuclear magnetic resonance studies of the glasses in the system Na2O-B2O3-SiO2. *J. Non-Cryst. Solids* **1978**, *27*, 363−380.

(94) Yun, Y. H.; Feller, S. A.; Bray, P. J. Correction and addendum to "Nuclear Magnetic Resonance Studies of the Glasses in the System Na2O-B2O3-SiO2". *J. Non-Cryst. Solids* **1979**, *33*, 273−277.

(95) Lee, S. K.; Stebbins, J. F. Nature of cation mixing and ordering in Na-Ca silicate glasses and melts. *J. Phys. Chem. B* **2003**, *107*, 3141−3148.

(96) Angeli, F.; Boscarino, D.; Gin, S.; Mea, G. D.; Boizot, B.; Petit, J. C. Influence of calcium on sodium aluminosilicate glass leaching behaviour. *Phys. Chem. Glasses* **2001**, *42*, 279−286.

(97) Molières, E.; Angeli, F.; Jollivet, P.; Gin, S.; Charpentier, T.; Majérus, O.; Barboux, P.; de Ligny, D.; Spalla, O. Chemical Durability of Lanthanum-Enriched Borosilicate Glass. *Int. J. Appl. Glass Sci.* **2013**, *4*, 383−394.

(98) Tilocca, A.; Cormack, A. N.; de Leeuw, N. H. The Structure of Bioactive Silicate Glasses: New Insight from Molecular Dynamics Simulations. *Chem. Mater.* **2007**, *19*, 95−103.

(99) Yamashita, H.; Inoue, K.; Nakajin, T.; Inoue, H.; Maekawa, T. Nuclear magnetic resonance studies of 0.139MO (or M'2O)·0.673SiO2·(0.188−x)Al2O3·xB2O3 (M=Mg, Ca, Sr and Ba, M'=Na and K) glasses. *J. Non-Cryst. Solids* **2003**, *331*, 128−136.

(100) Zheng, Q.; Potuzak, M.; Mauro, J. C.; Smedskjaer, M. M.; Youngman, R. E.; Yue, Y. Composition-structure-property relationships in boroaluminosilicate glasses. *J. Non-Cryst. Solids* **2012**, *358*, 993−1002.

(101) Allwardt, J. R.; Stebbins, J. F. Ca-Mg and K-Mg mixing around non-bridging O atoms in silicate glasses: An investigation using17O MAS and 3QMAS NMR. *Am. Mineral.* **2004**, *89*, 777−784.

(102) Delaye, J.-M.; Cormier, L.; Ghaleb, D.; Calas, G. Investigation of multicomponent silicate glasses by coupling WAXS and molecular dynamics. *J. Non-Cryst. Solids* **2001**, *293−295*, 290−296.

(103) Loewenstein, W. The distribution of aluminum in the tetrahedra of silicates and aluminates. *Am. Mineral.* **1954**, *39*, 92−96.

(104) Rimsza, J. M.; Du, J. Nanoporous silica gel structures and evolution from reactive force field-based molecular dynamics simulations. *npj Mater. Degrad.* **2018**, *2*, 18.

(105) Rimsza, J. M.; Du, J. Structural and Mechanical Properties of Nanoporous Silica. *J. Am. Ceram. Soc.* **2014**, *97*, 772−781.

(106) Charpentier, T.; Menziani, M. C.; Pedone, A. Computational simulations of solid state NMR spectra: a new era in structure determination of oxide glasses. *RSC Adv.* **2013**, *3*, 10550−10578. The Royal Society of Chemistry: Publisher